J. metamorphic Geol., 2002, **20,** 99–118

Thermodynamic modelling of the reaction muscovite + cordierite → Al_2SiO_5 + biotite + quartz + H_2O: constraints from natural assemblages and implications for the metapelitic petrogenetic grid

D. R. M. PATTISON,[1] F. S. SPEAR,[2] C. L. DEBUHR,[3] J. T. CHENEY[4] AND C. V. GUIDOTTI[5]

[1]*Department of Geology & Geophysics, University of Calgary, Calgary, AB, T2N 1 N4, Canada (pattison@geo.ucalgary.ca)*
[2]*Department of Earth and Environmental Sciences, Rensselaer Polytechnic Institute, Troy, NY, 12180, USA*
[3]*GR Petrology Consultants Inc., 4605 12 Street N.E., Calgary, AB, T2E 4R3, Canada*
[4]*Department of Geology, Amherst College, Amherst, MA, 01002, USA*
[5]*Department of Geological Sciences, University of Maine, Orono, ME, 04469–5790, USA*

ABSTRACT The reaction muscovite + cordierite → biotite + Al_2SiO_5 + quartz + H_2O is of considerable importance in the low pressure metamorphism of pelitic rocks: (1) its operation is implied in the widespread assemblage Ms + Crd + And ± Sil + Bt + Qtz, a common mineral assemblage in contact aureoles and low pressure regional terranes; (2) it is potentially an important equilibrium for pressure estimation in low pressure assemblages lacking garnet; and (3) it has been used to distinguish between clockwise and anticlockwise *P–T* paths in low pressure metamorphic settings. Experiments and thermodynamic databases provide conflicting constraints on the slope and position of the reaction, with most thermodynamic databases predicting a positive slope for the reaction. Evidence from mineral assemblages and microtextures from a large number of natural prograde sequences, in particular contact aureoles, is most consistent with a negative slope (andalusite and/or sillimanite occurs upgrade of, and may show evidence for replacement of, cordierite). Mineral compositional trends as a function of grade are variable but taken as a whole are more consistent with a negative slope than a positive slope. Thermodynamic modelling of reaction 1 and associated equilibria results in a low pressure metapelitic petrogenetic grid in the system K_2O–FeO–MgO–Al_2O_3–SiO_2–H_2O (KFMASH) which satisfies most of the natural and experimental constraints. Contouring of the Fe–Mg divariant interval represented by reaction 1 allows for pressure estimation in garnet-absent andalusite + cordierite-bearing schists and hornfelses. The revised topology of reaction 1 allows for improved analysis of *P–T* paths from mineral assemblage sequences and microtextures in the same rocks.

Key words: cordierite; metapelite; petrogenetic grid; phase equilibria; thermodynamics.

INTRODUCTION

The reaction involving the phases muscovite, cordierite, biotite, Al_2SiO_5 mineral (andalusite or sillimanite), quartz and hydrous fluid:

$$\underset{KAl_3Si_3O_{10}(OH)_2}{2\ Ms} + \underset{(Fe,Mg)_2Al_4Si_5O_{18}.nH_2O}{3\ Crd} = \underset{K(Fe,Mg)_3AlSi_3O_{10}(OH)_2}{2\ Bt} + \underset{Al_2SiO_5}{8\ And/Sil} + \underset{SiO_2}{7\ Qtz} + 3n\ H_2O \quad (1)$$

(balanced using idealized end members) is of considerable importance to metapelitic phase equilibria; (1) its operation is implied in the assemblage muscovite + cordierite + andalusite ± sillimanite + biotite + quartz, a common metapelitic assemblage in contact aureoles and low pressure regional terranes (Pattison & Tracy, 1991); (2) it is a key reaction in calibrating the petrogenetic grid for metapelites; (3) it is potentially an important equilibrium for pressure estimation in low pressure assemblages lacking garnet; (4) it has been used to distinguish between clockwise vs. anticlockwise *P–T* paths in low pressure metamorphic settings (e.g. Johnson & Vernon, 1995); and (5) its slope is sensitive to the thermodynamics of water in cordierite, making it an important test of different models.

The reaction is divariant in the model pelitic system K_2O–FeO–MgO–Al_2O_3–SiO_2–H_2O (KFMASH) (Fig. 1), such that its position and perhaps its slope varies according to the Fe/Mg ratio of the rock. Determining the slope and position of this reaction for

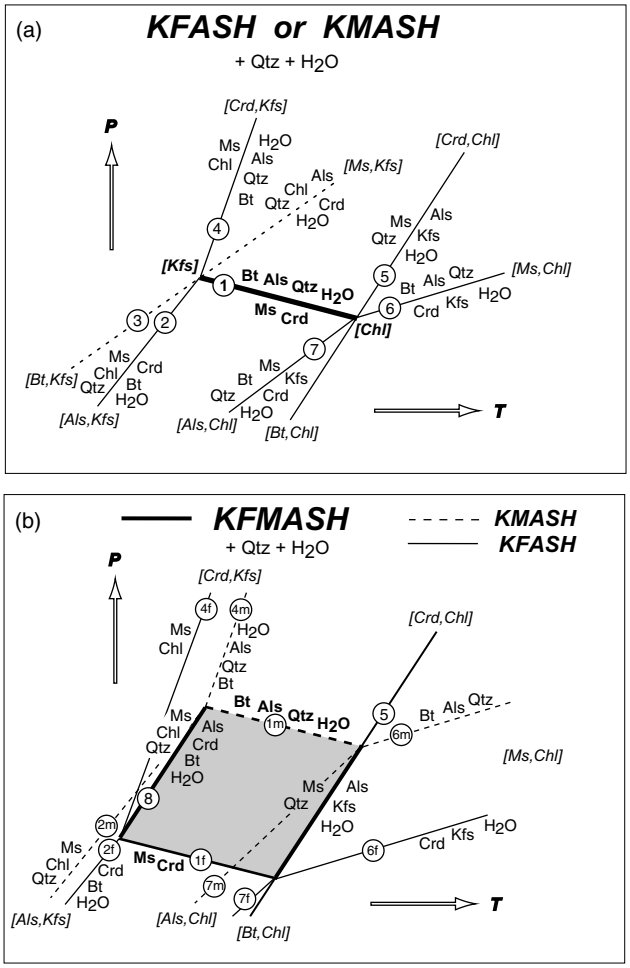

Fig. 1. Reactions and invariant points associated with reaction 1, $Ms + Crd \rightarrow Als + Bt + Qtz + H_2O$, in KFASH or KMASH (a) and in KFMASH (b). See text for discussion. Reaction 3, which may result in biotite-absent Als + Crd assemblages, is dashed in (a) and omitted in (b).

different Fe/Mg ratios has been problematic because of discrepancies among constraints from natural mineral assemblages, experiments and thermodynamic modelling.

This paper presents textural, modal and mineral compositional data from a large range of natural settings, especially contact aureoles, that bear on this question. We argue that although there is some ambiguity in interpreting the data, the data as a whole are more consistent with a negative slope for reaction 1 than a positive slope. We provide thermodynamic formulations of reaction 1 using the constraints provided by the natural assemblages which result in an acceptable fit to most of the relevant experimental data. The thermodynamic data are then used to calculate petrogenetic grids for graphitic and nongraphitic metapelites, and to contour reaction 1 for different Mg/(Mg + Fe) ratios. These results provide a means to estimate pressure in low pressure garnet-absent, andalusite + cordierite-bearing schists and hornfelses and allow improved interpretation of P–T paths from microtextures in the same rocks.

TOPOLOGY OF THE REACTION

Figure 1(a) shows schematically the topology of reaction 1 in relation to two important invariant points that it links in either of the K_2O–FeO–Al_2O_3–SiO_2–H_2O (KFASH) or K_2O–MgO–Al_2O_3–SiO_2–H_2O (KMASH) systems: the K-feldspar-absent invariant point [Kfs] and the chlorite-absent invariant point [Chl] (the square brackets indicate the phase(s) that are absent). The KMASH invariant points are known to be stable, whereas the KFASH invariant points may or may not be (see below).

In addition to reaction 1, the reactions associated with the [Kfs] invariant point that involve quartz and H_2O are:

$$Ms + Chl + Qtz \rightarrow Crd + Bt + H_2O \quad [Kfs,Als] \quad (2)$$

$$Chl + Als + Qtz \rightarrow Crd + H_2O \quad [Kfs,Ms,Bt] \quad (3)$$

$$Ms + Chl \rightarrow Als + Bt + Qtz + H_2O \quad [Kfs,Crd] \quad (4)$$

(abbreviations of Kretz, 1983; with Als = kyanite, andalusite or sillimanite).

In addition to reaction 1, the reactions associated with the [Chl] invariant point are:

$$Ms + Qtz \rightarrow Als + Kfs + H_2O \quad [Chl,Crd,Bt] \quad (5)$$

$$Bt + Als + Qtz \rightarrow Crd + Kfs + H_2O \quad [Chl,Ms] \quad (6)$$

$$Ms + Bt + Qtz \rightarrow Crd + Kfs + H_2O \quad [Chl,Als] \quad (7)$$

Reaction 5 is degenerate if the muscovite is assumed to have no Tschermak component, which is a reasonable first order simplification for this topological analysis.

When the system is expanded to KFMASH (Fig. 1b), the [Kfs] and [Chl] invariant points become univariant reactions. The [Kfs] univariant reaction is:

$$Ms + Chl + Qtz \rightarrow Crd + Als + Bt + H_2O \quad [Kfs] \quad (8)$$

whereas the [Chl] univariant reaction is the same as degenerate reaction 5. The univariant reactions in KFASH or KMASH become divariant fields in KFMASH, bounded by Fe- and Mg-end member curves (i.e. the KFASH and KMASH univariant curves). This assumes that the end member curves are not metastable relative to other competing equilibria. In Fig. 1(b), the divariant field for reaction 1 is shaded, and the bounding Fe- and Mg-end member curves are labelled 1f and 1m, respectively, a convention that is followed for the other reactions.

In Fig. 1, the slopes of the reactions other than reaction 1 are shown qualitatively to have moderate to

Fig. omitted in revision

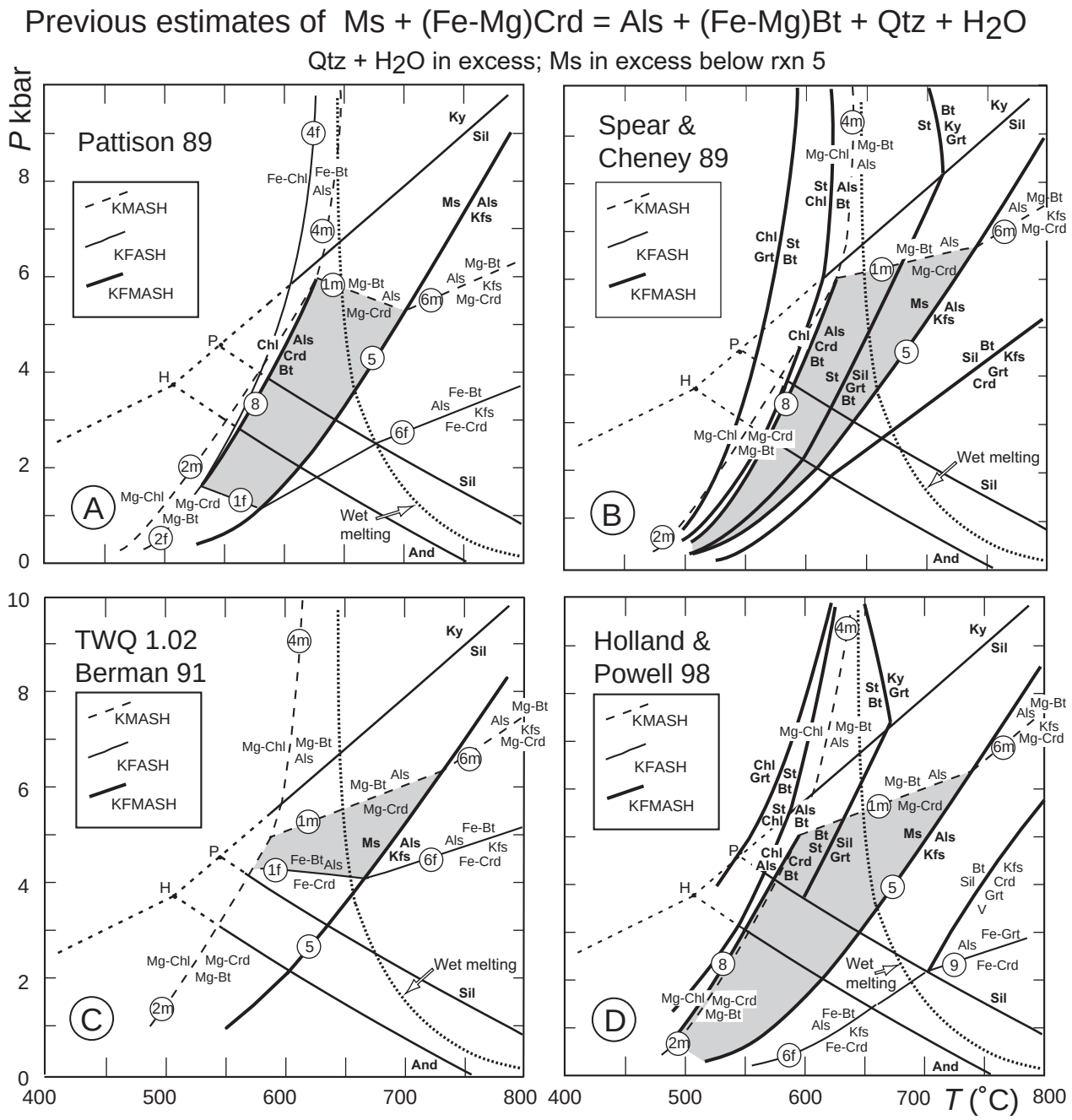

steep slopes, consistent with all experimental and thermodynamic constraints. Reaction 1 is shown to have a shallow negative slope, although Schreinemakers' constraints allows either a positive or negative slope.

EXPERIMENTAL CONSTRAINTS COMPARED TO THERMODYNAMIC MODELLING

Figure 2a shows the available experimental constraints for Mg-end member reaction 1m. The only two published studies, those of Seifert (1970) and Bird & Fawcett (1973), are mutually consistent and indicate a negative slope, although both studies reported experimental difficulties. Seifert noted small degrees of reaction progress and found that the phlogopite and muscovite inserted into the experimental capsules had become eastonitic and phengitic, respectively, during the course of the experiments. Bird & Fawcett (1973) reported a reversal of this reaction from a metastable corundum + quartz assemblage which raises some concerns about the result. Nevertheless, the agreement between the two studies is notable. In contrast, an abstract by Massonne (1988) reports preliminary experimental results (details unspecified) indicating a positive slope of about 9 °C bar^{-1} emanating from a point at around 5.5 kbar and 715 °C.

Figure 2(b) shows predictions of the slope and position of reaction 1m from the most recent thermodynamic data bases. Without exception they indicate a positive slope, although the positions of the curves vary a bit. Most of the curves are calculated assuming end member phlogopite and muscovite whereas the Holland & Powell (1998) curve is calculated for these minerals with a Tschermak component. Although the latter approach is recommended, the effect is small for reaction 1m because muscovite and Mg-biotite are on opposite sides of the reaction (see discussion in Pattison, 1989).

There are no experimental constraints on Fe-end member reaction 1f. However, there are experimental constraints on reaction 6f, which intersects reaction 5 to generate the [Chl] invariant point in KFASH, thus constraining the location of reaction 1f (see Figs 1 & 2). Figure 2a shows the experimental constraints of Holdaway & Lee (1977) on reaction 6f. They reported brackets for reaction 6f as 1.9–2.1 kbar at 642 °C and 2.6–2.8 kbar at 710 °C.

Holdaway & Lee study also investigated the Fe-end member reaction:

$$\text{Fe-Crd} \rightarrow \text{Alm} + \text{Sil} + \text{Qtz} \quad (9)$$

Mukhopadhyay & Holdaway (1994) re-investigated reaction 9 because they noted some hercynitic spinel in the cordierite and garnet starting material in the 1977 study, which they speculated might have reacted with quartz to produce cordierite and thus compromise inferences about cordierite stability with respect to Alm + Sil + Qtz. The 1994 placement of the reaction did indeed change from that in the 1977 study (stability of Fe-cordierite reduced by about 1 kbar), leading Holdaway & Mukhopadhyay (1993) to suggest that the experimental constraints on other equilibria in the 1977 study (in particular reaction 6f) should be discounted.

Unless there are other factors that were not reported in the 1977 study, we are less pessimistic about the results for reaction 6f. In contrast to reaction 9, which was monitored solely by cordierite consumption or growth, reaction 6f was monitored by both cordierite and biotite consumption/growth. Based on the data reported in Table 3 of Holdaway & Lee (1977) and only using experiments that

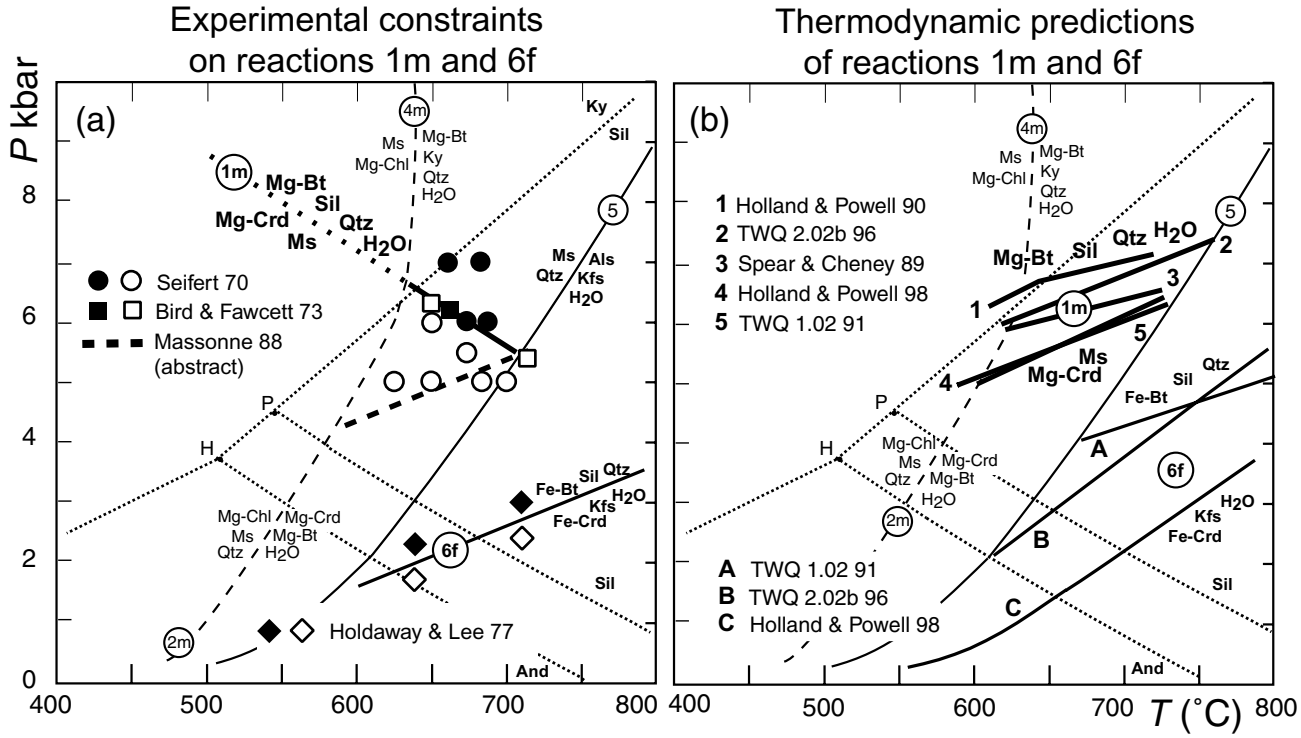

Fig. 2. Comparison of experimental data (a) and thermodynamically predicted positions (b) of reactions 1m and 6f. In the left hand diagram, the general trend of reactions 1m and 6f through the experimental brackets are shown by solid lines, with the exception of the Massonne (1988) curve for reaction 1m which is dashed. In (b), all curves except Holland & Powell (1998) were calculated assuming end member muscovite and phlogopite or annite, whereas the Holland & Powell (1998) curves are for micas with a Tschermak component. H and P — And = Sil curves and triple points of Holdaway (1971) and Pattison (1992), respectively. TWQ 1.02 — Berman (1991). TWQ 2.02b — Berman & Aranovich (1996) and Aranovich & Berman (1997).

show unambiguous evidence of *both* cordierite growth and biotite consumption or *both* cordierite consumption and biotite growth, we suggest that the brackets may reasonably be widened to 1.7–2.3 kbar at 642 °C and 2.4–3.0 kbar at 710 °C, not markedly different from the original brackets. These latter brackets are the ones shown in Fig. 2(b).

Figure 2(b) shows predictions of the slope and position of reaction 6f from the most recent thermodynamic data bases. Although the slopes are similar, the positions are significantly different. Direct comparison between the curves is complicated because the two TWQ curves are calculated for end member annite whereas the Holland & Powell (1998) curve is calculated for Fe-biotite with a Tschermak component, but this difference is modest and does not reconcile the large discrepancies shown in Fig. 2(b).

CONSTRAINTS FROM NATURE

Given the contradictory experimental and thermodynamically predicted results for reaction 1, we have turned to well studied natural settings to see if there are any consistent patterns that might shed light on the problem. Implicit in this approach is the assumption that it is valid to compare mineral reactions in nature with those conducted in simpler chemical systems in the lab, which are the basis for the thermodynamic models. We discuss this issue in detail with respect to reaction 1 at the end of the Appendix.

In our evaluation of natural assemblages, we follow Pattison & Tracy (1991) and Pattison *et al.* (1999) in emphasising the importance of constraints from contact aureoles around single intrusions for two main reasons. First, the thermal history is relatively simple, thereby eliminating complications from polymetamorphism such as encountered in many regional low pressure terranes; and second, the thermal pulse and decay is relatively rapid (generally <1 Ma), such that both the prograde P–T path for individual rocks as well as the metamorphic field gradient can be assumed to be sensibly isobaric rather than involving significant variation in both pressure and temperature.

The second point is important because most agree that reaction 1 has a shallow P–T slope, whether positive or negative (Fig. 2). Possible complications in this assumption include: nonhydrostatic stress associated with pluton emplacement, as may be indicated by tectonic foliations in some aureoles; dragging up or down of country rocks adjacent to the margins of intrusions during emplacement; magmatic loading; post-emplacement tilting; and faulting. Brace *et al.* (1970), Rutter (1976), Carmichael (1978) and Shimizu (1995) have shown that nonhydrostatic stress is unlikely to exceed about 100 bar and can thus be ignored, especially in rocks undergoing recrystallization due to reactions. Upward or downward flow of country rock adjacent to intrusions implies a diapiric emplacement mechanism which finds limited support in nature (see Brown *et al.*, 1995 and references therein) and in any case does not apply to most of the aureoles considered below. Magmatic loading (emplacement of magma above the present level of erosion, leading to pressure increase in the aureole) is discussed separately below. Tilting would have to be extreme in order to effect significant pressure variations across aureoles which are typically less than 2 km wide (Pattison & Tracy, 1991). We have assumed that faulting was considered by the authors of the various studies referenced. In summary, while some degree of pressure variation during contact metamorphism around intrusions cannot be ruled out, it seems that isobaric heating is a good first order assumption unless there are obvious geological features to suggest otherwise.

The theoretical basis for our evaluation is illustrated in Fig. 3, which shows a schematic P–T pseudosection (Hensen, 1971) and corresponding schematic isobaric T-$X_{\mathrm{Fe\text{-}Mg}}$ diagram for the two competing situations in which reaction 1 has a positive or negative slope. For an isobaric prograde P–T path, if the P–T slope of reaction 1 is negative (Fig. 3a), Als + Bt is produced at the expense of Ms + Crd and both minerals become more Mg-rich as grade increases. If the slope of reaction 1 is positive (Fig. 3b), Ms + Crd is produced at the expense of Als + Bt and both minerals become more Fe-rich as grade increases.

The evidence used to test the two competing hypotheses includes mapped isograd patterns, modal variations as a function of grade, textures and mineral composition variations. We examine low pressure andalusite-sillimanite settings first, followed by rarer higher pressure sillimanite-only settings and lastly controversial kyanite + cordierite-bearing localities.

Isograd patterns and modal variations in andalusite-sillimanite settings

Prograde sequences in contact aureoles and regional low pressure settings in which the mineral assemblage involved in reaction 1, Ms + Crd + And + Bt + Qtz, is developed are abundant (Pattison & Tracy, 1991). However, in most contact metamorphic settings, the metamorphic field gradient and P–T path followed by individual rocks passes through either reactions 2 and 8, or 4 and 8, prior to reaction 1 (see Figs 1 & 3). In either case, isograds marking the first occurrence of andalusite and cordierite occur downgrade of reaction 1, meaning there is no special new mineral association (i.e. isograd) indicative of reaction 1. Examples of this situation are the Bugaboo aureole, B.C. (Pattison & Jones, 1993; DeBuhr, 1999), Onawa aureole, Maine (Symmes & Ferry, 1995), McGerrigle aureole, Quebec (van Bosse & Williams-Jones, 1988), and several others listed in Pattison & Tracy (1991).

An exception is the Ballachulish aureole, Scotland (Pattison & Harte, 1997). In the graphitic Ballachulish Slate lithology, hornfelsic Ms + Crd + Bt + Qtz assemblages pass upgrade along strike in the same stratigraphic unit into hornfelsic Ms + Crd + And + Bt + Qtz assemblages, with an andalusite isograd separating the two metamorphic zones (Pattison & Harte, 1985, 1991). Pattison (1989) interpreted the andalusite isograd to be the result of reaction 1 which, assuming an isobaric metamorphic field gradient, implies that the slope is negative. The inferred P–T path for this interpretation is shown by the dashed lines labelled 'B' in Fig. 3(a). Textural evidence (see below) supports this interpretation. Other localities that indicate a similar isograd sequence include the Strath Ossian aureole (Key *et al.*, 1993), in which andalusite is developed upgrade of the assemblage Ms + Crd + Bt + Qtz, and the regional contact metamorphic setting near Whitehead Harbour, Nova Scotia (Raeside *et al.*, 1988).

Fig. omitted in revision

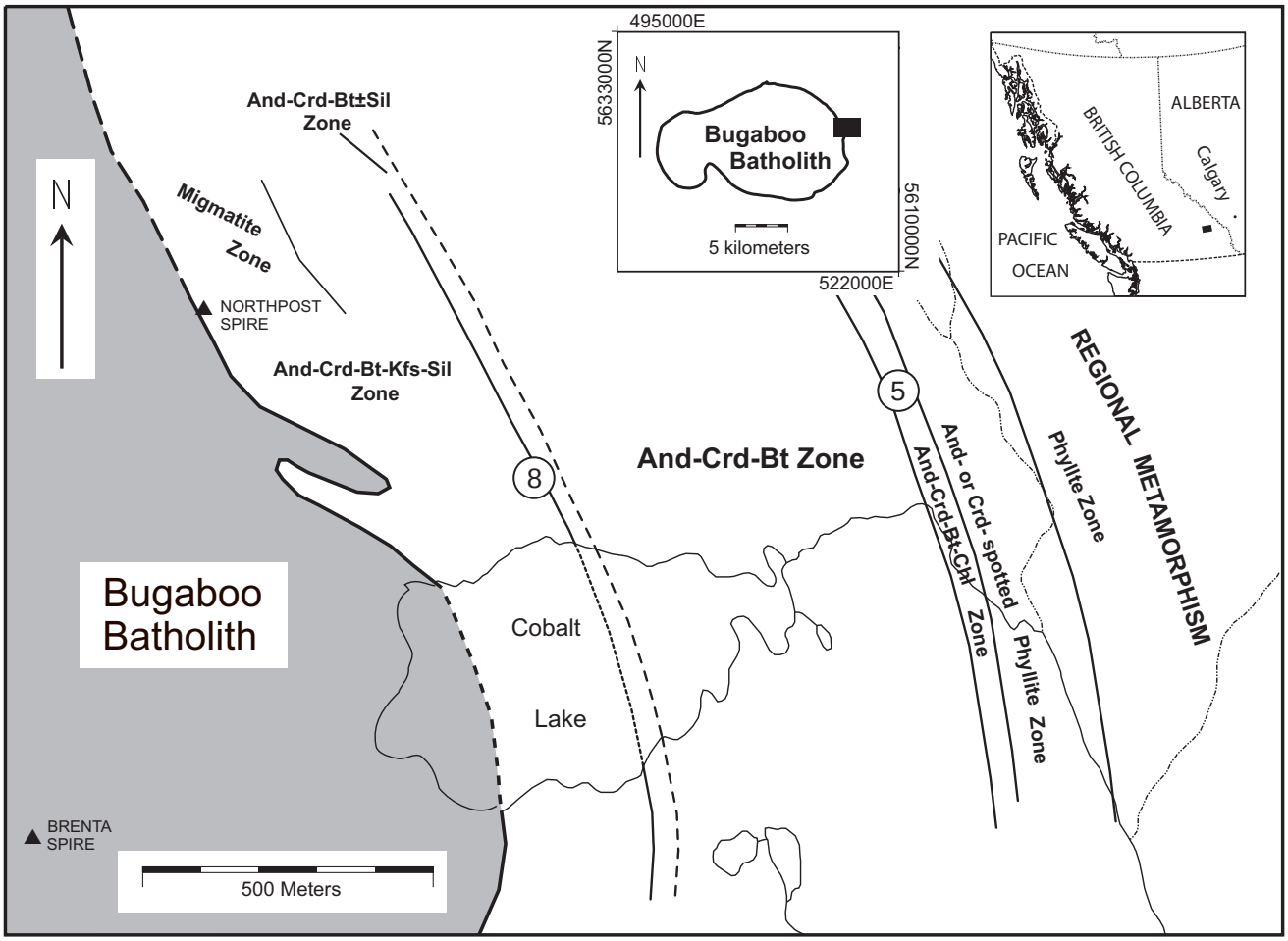

Fig. omitted in revision

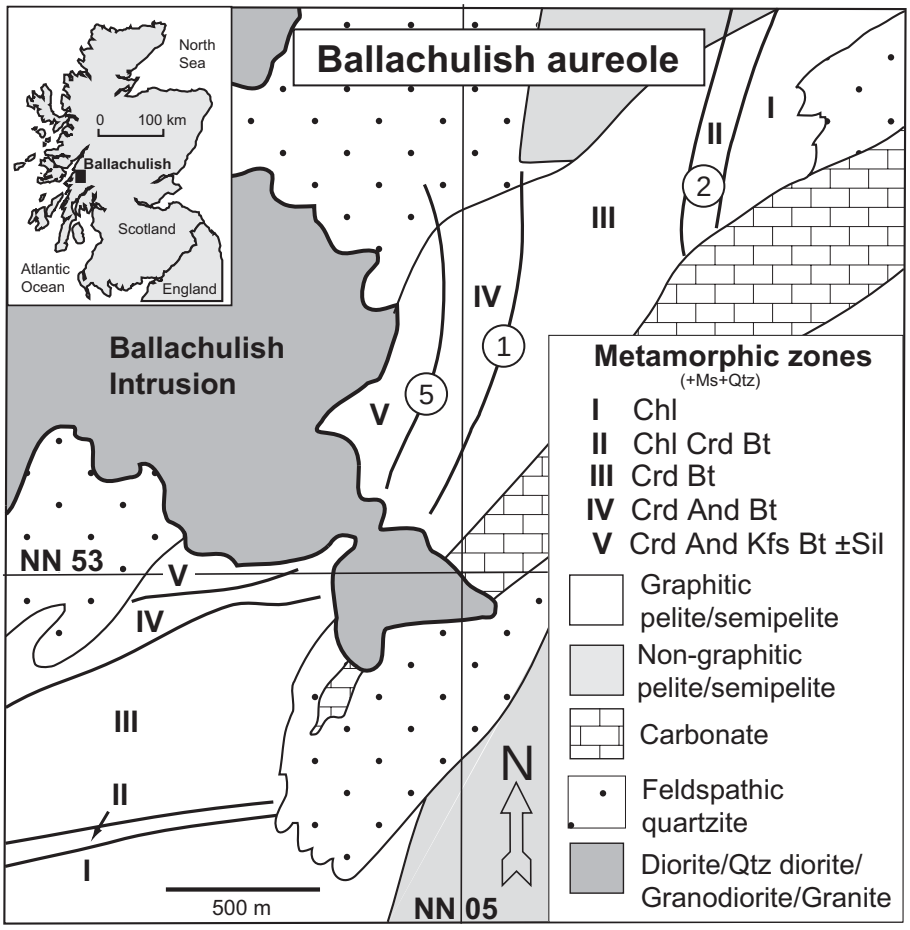

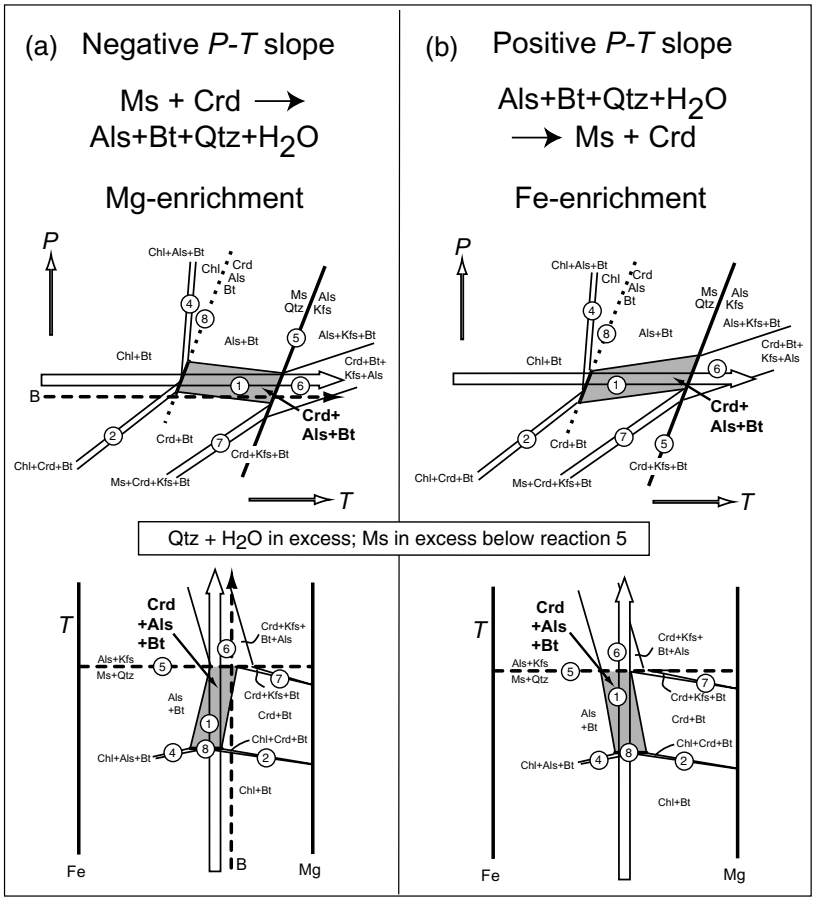

Fig. 3. Schematic P–T and corresponding isobaric T–$X_{Fe\text{-}Mg}$ diagrams for the two competing situations in which reaction 1 has a negative slope (a) or positive slope (b). The inferred direction of reaction and corresponding sense of Fe- or Mg-enrichment assumes a prograde P–T path (see text for discussion).

Variations in modal mineralogy as a function of grade have been rarely reported in the above localities but are available for the Bugaboo aureole (Fig. 4). Although the modes are strongly dependent on the bulk composition of the rocks and show a somewhat erratic pattern, there is a general trend in which And + Bt increases going upgrade in the aureole relative to Ms + Crd.

Textures in andalusite-sillimanite aureoles

Figure 5(a–h) shows photomicrographs of textures in the assemblage Ms + Crd + And ± Sil + Bt + Qtz from some of the above localities. Figure 5a shows euhedral-subhedral andalusite surrounded by biotite from the Ballachulish aureole, consistent with production of And + Bt at the expense of Ms + Crd in the matrix. Figure 5b shows And + Bt + Qtz in a pressure shadow between pulled apart cordierite porphyroblasts from the aureole of the South Mountain Batholith, Nova Scotia (localities in Raeside & Jamieson, 1992), indicating that And + Bt + Qtz post-dates the cordierite.

Figure 5(c–g) show some common textures from the Bugaboo aureole, B.C. (Pattison & Jones, 1993; DeBuhr, 1999) (Fig. 4). Figure 5c shows inclusion-rich andalusite porphyroblasts from the Chl + Crd + And + Bt zone, which occurs at the low grade end of the Crd + And + Bt zone (the latter containing the reaction 1 assemblage). In comparison, Fig. 5d shows andalusite at higher grade from the middle of the Crd + And + Bt zone showing a thin clear rim overgrowing an inclusion rich core. The core shows a distribution and grain size of inclusions like that in Fig. 5a. The matrix surrounding the andalusite porphyroblast and partially included in its clear rim is markedly coarser than in the inclusion rich core, consistent with prograde matrix coarsening and growth of andalusite. A ragged cordierite poikiloblast occurs beside the andalusite. Figure 5e is an example of a cordierite-rich sample containing thin 'films' of andalusite between ovoid cordierite poikiloblasts, the only place that andalusite occurs in these samples and which we interpret to indicate andalusite growth after cordierite. Figure 5f shows zones of And + Bt + Qtz cross-cutting cordierite crystals. The andalusite overgrows a crenulated fabric that is distinct from, and post-dates, the more planar fabric in the cordierite crystal defined by aligned fine grained inclusions. Figure 5g shows cordierite porphyroblasts wrapped by a mica-rich matrix which is overgrown by andalusite, and andalusite has additionally replaced the cordierite.

All of the textures in Fig. 5(a–g) provide evidence for the development of andalusite at the expense of cordierite. Other contact aureoles that provide textural evidence of the same relationship include the Santa Rosa aureole, Nevada (Compton, 1960; p. 1406) and the Cupsuptic aureole, Maine (Ryerson, 1979; p. 84).

These observations can only be translated into information about the slope of reaction 1 if the metamorphic field gradient and P–T path of individual samples in the aureoles is known, and the textures can be identified as being due to prograde or retrograde processes. As discussed earlier, we consider an isobaric metamorphic field gradient and P–T path to be a reasonable inference in the absence of evidence suggesting otherwise. Magmatic loading might account for the development of And + Bt at the expense of Ms + Crd if the loading were significant and occurred during the relatively short period of time when the rocks were being heated or were still relatively hot, but to infer this process in all the aureoles which show these textures seems rash without further evaluation of each aureole. Upward drag of country rocks by a rising intrusion, resulting in an apparent increase in pressure going upgrade in the aureole, does not fit with the field observations in at least the Ballachulish, Bugaboo and South Mountain aureoles.

If the slope of reaction 1 is negative, the development of andalusite at the expense of cordierite can be ascribed simply to prograde

isobaric heating through reaction 1 as illustrated in Fig. 3a. If the slope of reaction 1 is positive, the textures imply retrograde metamorphism without significant pressure decrease (reverse of the arrow in Fig. 3b). Interestingly, retrograde passage through reaction 1 with a positive slope would result in dehydration (rather than hydration) because H_2O occurs on the andalusite-bearing side of the reaction. Although a retrograde origin for the textures merits careful consideration, we question whether the kinetics of reaction during falling temperature would be sufficient to account for the full extent and range of textural and modal features described from the various aureoles. In addition, we would expect at least as widespread development of prograde textures involving cordierite formation at the expense of andalusite owing to the more efficient kinetics during heating, for which there is no evidence. Lack of prograde reaction progress through reaction 1 with a positive slope, due to water being a reactant, seems unlikely in a pile of otherwise dehydrating pelites in an aureole, especially if there is any fluid circulation driven by the heat of the intrusion. Metamorphic settings in which water-consuming, cordierite-producing reactions have proceeded, either during heating (Pattison & Harte, 1991) or during decompression (several examples in Pattison *et al.*, 1999), implies that water, if it is around, finds its way to the sites of reaction. In summary, we prefer the simple interpretation of a prograde origin for the textures and thus a negative slope for reaction 1.

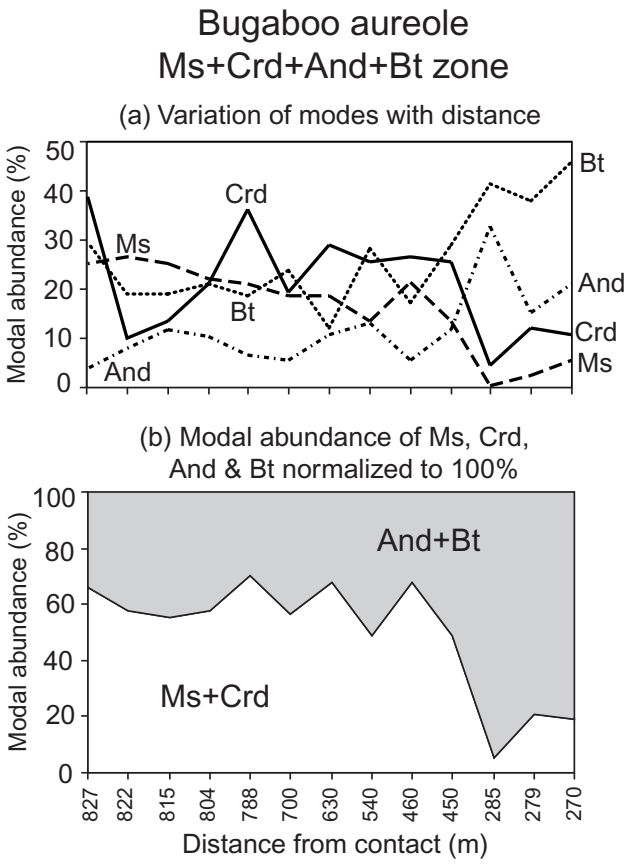

Fig. 4. Modal mineralogical variations in the Bugaboo aureole as a function of distance from the intrusive contact. (a) Absolute modal abundances of muscovite, cordierite, biotite and andalusite. (b) Normalized abundances of Ms + Crd vs. And + Bt.

Textures in andalusite-sillimanite regional terranes

Regional terranes that show textural evidence for Ms + Crd → And + Bt include: the regional contact aureole near Whitehead Harbour, Nova Scotia (Raeside *et al.*, 1988), in which andalusite overgrows a matrix fabric that wraps cordierite porphyroblasts; the Cooma aureole, New South Wales, where Vernon (1988) showed a progression of microtextures with increasing grade that demonstrated the development of And + Bt at the expense of Ms + Crd; the Mary Kathleen fold belt, Queensland, where Reinhardt & Rubenach (1989) and Reinhardt (1992) used microtextures to distinguish two different andalusite-forming reactions, the higher grade of which they interpreted to be Ms + Crd → And + Bt; and localities in the Slave province, Northwest Territories (Thompson, 1978; Bégin, personal communication 1994), in which andalusite post-dates and in some cases replaces cordierite in Ms + Crd + And ± Sil + Bt + Qtz assemblages. Although the regional metamorphic localities indicate prograde progress of the reaction Ms + Crd → And + Bt, they provide poorer constraints than the aureole settings on the slope of reaction 1 because there are greater uncertainties in the *P–T* slope of the metamorphic field gradient and the *P–T* paths of individual rocks. Several of the studies argued for pressure increase accompanying an increase in grade, which could allow for progress of reaction 1 whether it has a shallow positive or negative slope.

Mineral composition variations in andalusite-sillimanite settings

Figure 6 shows prograde variations in Mg/(Mg + Fe) of cordierite and biotite in the assemblage Ms + Crd + And + Bt + Qtz from four contact metamorphic localities and one regional locality: the Cupsuptic aureole, Maine (Ryerson, 1979); the McGerrigle aureole, Quebec (van Bosse & Williams-Jones, 1988); the Tono aureole, Japan (Okuyama-Kusunose, 1993); the Onawa aureole, Maine (Symmes & Ferry, 1995); and the W. Maine regional setting (Guidotti *et al.*, 1986). Compositional data from other aureoles are listed in Table 1.

Fig. 5. Photomicrographs of textures in the assemblage Ms + Crd + Als + Bt from different localities. See text for discussion. (a) Ballachulish aureole. Euhedral andalusite surrounded by biotite in cordierite-bearing matrix. (b) South Mountain Batholith aureole. Intergrown andalusite, biotite and quartz in a pressure shadow between pulled apart cordierite crystals. (c) Bugaboo aureole, Cobalt Lake area (E margin of complex). Andalusite and cordierite from the low grade margin of the And + Crd + Bt zone. The inclusions in the andalusite are of a similar grain size to those in the matrix, and define a similar fabric. (d) Bugaboo aureole, Cobalt Lake area. Andalusite and cordierite from the upper grade part of the And + Crd + Bt zone. The inclusions in the middle of the andalusite are of a similar texture and grain size to those in the andalusite in Fig. 5(c), but the surrounding matrix has a coarser grain size and has a fabric at a high angle to the one preserved in the andalusite grain. The andalusite has a clear rim that locally includes or partially overgrows biotite grains from the matrix. These textures are consistent with prograde matrix coarsening and andalusite growth. A ragged cordierite porphyroblasts is also visible. (e) Bugaboo aureole, Cobalt Lake area. Interstitial andalusite between two cordierite porphyroblasts from the middle of the And + Crd + Bt zone. (f) Bugaboo aureole, Iceberg lake area (N margin of complex). Andalusite and biotite cross-cutting and overgrowing the margins of cordierite. Inclusions in the andalusite reveal a coarse, crenulated fabric that is distinct from the fine grained, linear fabric in the cordierite. Both textures indicate growth of andalusite after cordierite. (g) Bugaboo aureole, Kickoff Meadows area (SW margin of complex). Andalusite overgrowing a matrix fabric that wraps pinitized chordate porphyroblasts. The andalusite has locally replaced the cordierite. (h) W Maine. Intergrown sillimanite, biotite and quartz in the pressure shadow of a cordierite porphyroblast.

Figure 5

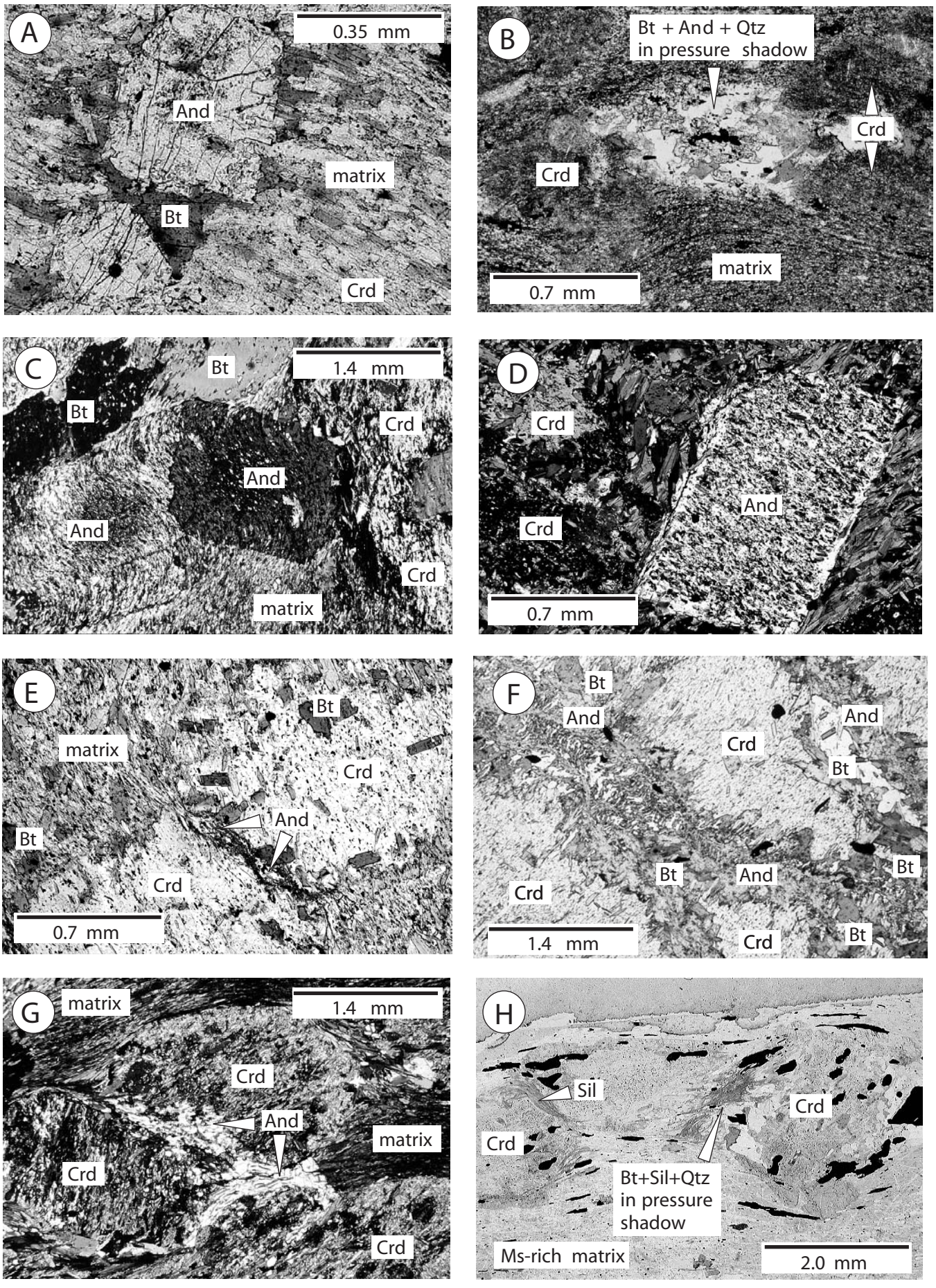
A
0.35 mm
And
matrix
Bt
Crd
B
Bt + And + Qtz
in pressure shadow
Crd
Crd
matrix
0.7 mm
C
Bt
1.4 mm
Bt
Crd
And
And
Crd
matrix
D
Crd
And
Crd
0.7 mm
E
Bt
matrix
Crd
And
Bt
Crd
0.7 mm
F
Bt
And
And
Crd
Bt
Bt
And
Bt
Crd
1.4 mm
Crd
Bt
G
matrix
1.4 mm
Crd
And
matrix
Crd
Crd
H
Sil
Crd
Crd
Bt+Sil+Qtz
in pressure
shadow
Ms-rich matrix
2.0 mm

Although the data are somewhat scanty, the trend consistently seems to be one of weak Mg-enrichment as grade increases.

The situation is less simple in two localities where there has been more extensive sampling: the Ballachulish aureole (Fig. 7) and the Bugaboo aureole (Fig. 8). At Ballachulish (Fig. 7), the pattern is complicated by samples which contain relatively F-rich (>1.2 wt% F) and correspondingly anomalously Mg-rich biotite (see Guidotti, 1984 for a discussion of this effect). Ignoring these samples, there is still no clearly discernible trend to either Fe-richer or Mg-richer compositions as grade increases. In Fig. 7, biotite generally becomes Mg-richer with increasing grade in the assemblage Ms + And + Crd + Bt, but cordierite if anything becomes somewhat Fe-richer. We do not think that the apparent prograde trend in these few samples to a narrowing of K_D (Fe–Mg) Crd-Bt is significant, based on the more extensive study of Crd–Bt Fe–Mg partitioning in the aureole as a whole (Pattison, 1987). The overall pattern is puzzling because the distribution of reactants and products of reaction 1 and the textures both suggest development of andalusite + biotite at the expense of cordierite as grade increases which, if due to reaction 1, *requires* that the minerals become more Mg-rich, regardless of the slope of the reaction and the metamorphic field gradient. Core-rim analysis of cordierite from two samples (Pattison & Harte, 1991) showed a weak trend to Mg-enrichment ($\Delta Mg/(Mg+Fe) = 0.02$), consistent with the textural evidence.

At Bugaboo (Fig. 8), the situation is no clearer. Looking at the data as a whole, biotite shows no significant trend to Fe- or Mg-enrichment as grade increases, whereas cordierite shows a weak trend to Fe-richer compositions as grade increases. On the other hand, there is a break at about 500 m which separates lower grade and higher grade domains of weak prograde Mg-enrichment of both minerals. DeBuhr (1999) found no mineralogical, chemical or textural explanations for this apparent break. The compositional data as a whole therefore appear to be inconsistent with the modal and textural evidence (Figs 4 & 5) indicating development of andalusite at the expense of cordierite as grade increases, assuming that the textures are due to progress of reaction 1.

To test the possibility that the textures might be due to reactions involving minor (non-KFMASH) elements or mineral compositional changes other than Fe-Mg, DeBuhr (1999) searched for correlations between Mg/(Mg + Fe) in cordierite and biotite and all nontrivial minor elements or mineral exchange vectors: Mn in cordierite, Ti in biotite, K and Na in muscovite and biotite, F in biotite, and Al and Si content of muscovite and biotite (the latter recording variation in Tschermak content of the micas). The only significant correlation was between Mg/(Mg + Fe) of cordierite and biotite and the bulk Mg/(Mg + Fe) ratio of the rocks. This correlation is at odds with predictions from equilibrium thermodynamics because, for a given mineral assemblage at a fixed or some small range of *P–T*, variations in bulk composition should cause different modal proportions of the minerals rather than different mineral compositions.

The results at Bugaboo may point to sluggish kinetics of equilibration, with the Mg/(Mg + Fe) compositions of cordierite and biotite perhaps being retained from their initial formation from lower grade chlorite-consuming reactions like reactions 2 or 8 (DeBuhr, 1999). Compositional mapping of the samples shown in Fig. 5d and f shows that individual cordierite and biotite crystals show no internal zoning in Fe/Mg and that biotite crystals show little spatial variation in Fe/Mg as a function of textural association (e.g. at differing distances in the matrix from cordierite or andalusite porphyroblasts, as inclusions within cordierite and andalusite porphyroblasts compared to the matrix, or intergrown with late-looking andalusite). These features imply rapid Fe-Mg exchange between biotite and cordierite and perhaps a low closure temperature for the exchange, which could contribute to the ambiguity of the results in Fig. 8. Variations in a_{H_2O} or Fe^{2+}/Fe^{3+} might induce slight variations in the Mg/(Mg + Fe) of the minerals (Cheney & Guidotti, 1979), further masking what are in any case subtle compositional trends.

In summary, whereas most of the compositional data in Table 1 and Fig. 6 indicate weak Mg-enrichment in the assemblage Ms + Crd + And + Bt + Qtz as grade increases, the two most detailed data sets (Ballachulish and Bugaboo) are ambiguous for reasons

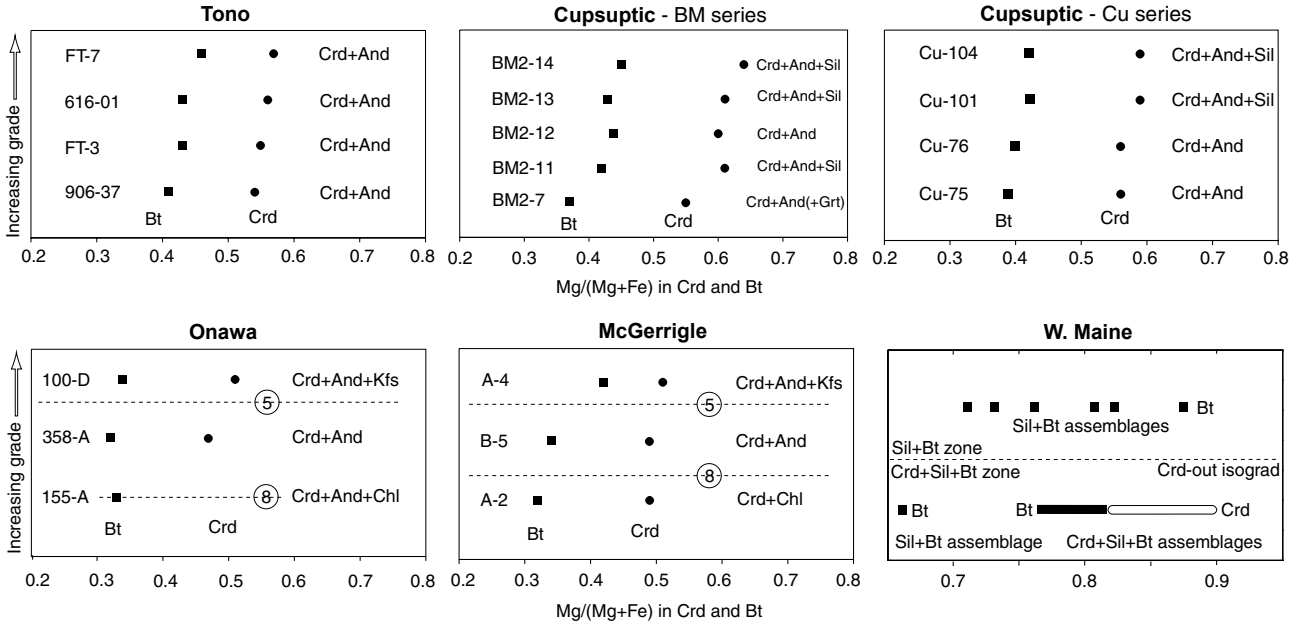

Fig. 6. Variation of Mg/(Mg + Fe) in coexisting cordierite and biotite as a function of assemblage and grade in localities from the literature (references listed in Table 1). All mineral assemblages contain Ms + Bt + Qtz. Data for W Maine come from Guidotti & Cheney (unpublished data). The sample number and assemblage are listed beside each rock's biotite and cordierite analyses. Numbered reaction isograds are shown for the Onawa and McGerrigle aureoles, whereas the unnumbered cordierite-out isograd (interpreted to be due to reaction 1 — see text) is shown for W Maine. For the W Maine data, a range of values is shown for cordierite and biotite in the assemblage Ms + Crd + Sil + Bt because the samples were collected close together.

Table 1. Mg/(Mg + Fe) of biotite and cordierite in Ms + Crd + Chl + Qtz + Als + Bt (reaction 8) assemblages and Ms + Crd + Kfs + Qtz + Als + Bt (reaction 5) assemblages.

Locality	Facies series C — contact R — regional	Graphitic?	Ms + Chl + Qtz + Crd + Bt + Als (R8)			Ms + Qtz + Als + Kfs + Bt + Crd (R5)			Difference (R5 − R8)	
			Al_2SiO_5	Bt	Crd	Al_2SiO_5	Bt	Crd	Bt	Crd
Comrie	C–1a	N	A	–	–	A	0.31	altered	–	–
Duluth	C–1a	N	A	–	–	A	<0.34	<0.49	–	–
Stawell	C–1a	N	A	–	–	A	<0.35	<0.50	–	–
Arthursleigh	C–1a	N	A	–	–	A	<0.37	<0.48	–	–
Ballachulish	C–1b	N	A	<0.30	<0.46	A	0.35–0.41	0.49–0.50	>0.05	>0.03
Ballachulish		Y	A	<0.43	<0.55	A	>0.46	>0.54	>0.03	> −0.01
Liberty Hill	C–1b	N	A	–	–	A	<0.35	<0.56	–	–
Etive	C–1b	N	A	–	–	A	0.40	0.56	–	–
Onawa	C–1c	Y/N*	A	0.32–0.33	0.47	A	>0.34	>0.52	>0.01	>0.05
McGerrigle	C–1c	N	A	<0.34	<0.49	A	0.42	0.51	>0.08	>0.02
Tono	C–1c	Y	A	0.40–0.41	0.54	A	>0.46	>0.57	>0.05	>0.03
Lexington N	C–1c/2a	N	A	–	–	A/S	>0.31	>0.46	–	
Bugaboo	C–1c/2a	N	A	0.41–0.43	0.53–0.59	A/S	0.40–0.43	0.56–0.59	−0.03–0.02	−0.03–0.06
Cupsuptic	C–2a	N	A	<0.39	<0.57	S	>0.43	>0.59	>0.04	>0.02
Kiglapait	C–2a	N	A	0.38–0.44	<0.59	S	>0.41	>0.56	−0.03 to >0.03	> −0.03
Kiglapait		Y	A	–	–	S	0.60	0.63–0.67	–	–
Hidaka	R–2a	Y	A	<0.44	<0.62	S	<0.46	0.62–0.63	>0.02?	>0.00
Buchan	R–2a/b	N	A	<0.40	<0.54	S	–	–	–	–
Panamint	R–2b	N	A	0.52	0.65	S	–	–	–	–
Black Hills	R–2b	Y	A	0.60	0.74	S	–	–	–	–
Mt Isa	R–2b	N	A	<0.80	<0.89	S	–	–		
W Maine	R–3	Y	S	<0.76	<0.82	S	>0.87	–	>0.05	–
Truchas	R–2, 3 or 4?	N	K?	0.70–0.73	0.85–0.86	S	–	–	–	–
Whetstone Lake	R–4?	N	K?	<0.86	<0.95	S	–	–	–	–
								Mean:	**>0.04**	**>0.02**

*Gr is variably present in reaction 8 assemblages but not in reaction 5 assemblages.

References

Facies series: Pattison & Tracy, 1991 and Pattison *et al.*, 1999.

Comrie — Pattison & Voordouw (unpubl.); Duluth — Labotka (1983), Labotka *et al.* (1981, 1984); Stawell — Xu (1993), Xu *et al.* (1994); Arthursleigh — Chenhall *et al.* (1988); Ballachulish — Pattison (1987, 1989), Pattison & Harte (1991, 1997, 2001); Liberty Hill — Speer (1981); Etive — Droop & Treloar (1981); Onawa — Symmes & Ferry (1995); McGerrigle — van Bosse & Williams-Jones (1988); Tono — Okuyama-Kusunose (1993); Lexington N — Dickerson & Holdaway (1989); Bugaboo — DeBuhr (1999); Cupsuptic — Ryerson (1979); Kiglapait — Speer (1982); Hidaka — Shiba (1988); Buchan — Hudson (1980); Panamint — Labotka (1981); Black Hills — Helms & Labotka (1991); Mt Isa — Rubenach (1992); W Maine — Guidotti *et al.* (1975), Guidotti & Cheney (unpubl.); Truchas — Grambling (1981); Whetstone Lake — Carmichael *et al.* (1978).

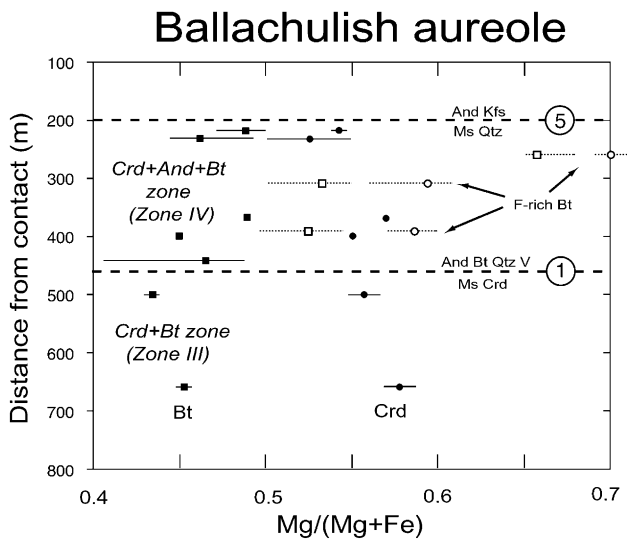

Fig. 7. Variation of Mg/(Mg + Fe) in coexisting cordierite and biotite as a function of assemblage and grade in the Ballachulish aureole, Scotland (Pattison, 1987 and unpublished data). Fe-rich biotite means that it contains more than 1.2 wt% Fe. Square symbols — biotite. Dots — cordierite. Bars represent the range of measured analyses.

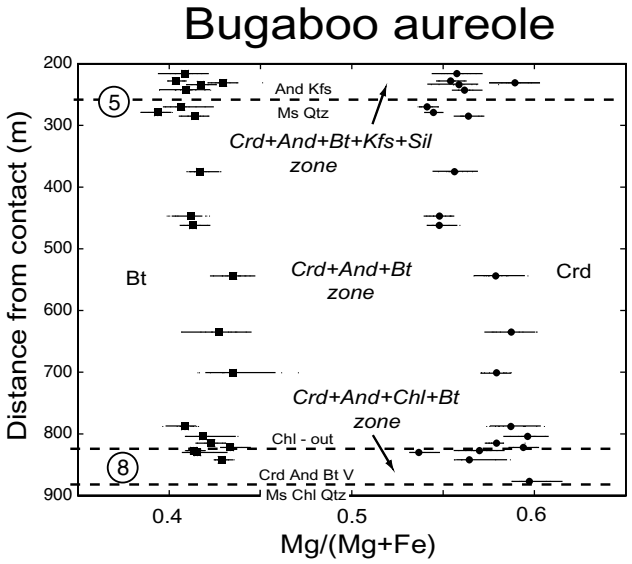

Fig. 8. Variation of Mg/(Mg + Fe) in coexisting cordierite and biotite as a function of assemblage and grade in the Bugaboo aureole, BC (DeBuhr, 1999). Square symbols — biotite. Dots — cordierite. Bars represent the range of measured analyses.

that are unclear. Taking all of the data together, the data show no indication of an overall trend to Fe-enrichment. We therefore conclude that the compositional data as a whole do not contradict the textural and modal evidence in support of a negative *P–T* slope for reaction 1, even if they do not provide clear support.

Sillimanite-only settings

Higher pressure prograde sequences that contain Ms + Crd + Sil + Bt + Qtz, without any andalusite, are rare because this assemblage is only developed at these pressures in relatively Mg-rich bulk compositions. The most notable and well studied example where this situation pertains is in W Maine, where metamorphosed graphite- and sulphide-bearing rocks of the Smalls Falls Formation have resulted in Mg-rich bulk compositions that develop cordierite (Guidotti *et al.*, 1986). In the more abundant 'normal' pelitic rock compositions interbedded with the cordierite-bearing Smalls Falls Formation rocks, staurolite-bearing assemblages give way upgrade to Sil + Bt ± Grt assemblages. The metamorphic pressure is 4.5 ± 1 kbar (Holdaway *et al.*, 1997).

The lowest grade occurrence of cordierite in the Small Falls Formation is in the mineral assemblage Ms + Chl + Crd + Bt within the Upper Staurolite Zone (Guidotti *et al.*, 1975). The most likely reaction accounting for development of cordierite in this assemblage is reaction 2. At higher grades, cordierite occurs in the assemblage Ms + Crd + Sil + Bt within the Lower and Upper Sillimanite Zones. No assemblages have been found with the model univariant assemblage Ms + Chl + Crd + Sil + Bt (corresponding to reaction 8), although textural evidence for two episodes of cordierite growth in the Ms + Crd + Sil + Bt assemblages suggests progress of reaction 8 following the inferred main growth of cordierite by reaction 2.

Guidotti *et al.* (1986) showed a cordierite-out isograd that occurs within the Upper Sillimanite Zone (Ms + Grt + Sil + Bt). Across the isograd, Ms + Crd + Sil + Bt assemblages give way upgrade to Ms + Sil + Bt assemblages. Textural evidence for reaction of cordierite to Sil + Bt is provided in Fig. 5h, in which Bt + Sil occur in the pressure shadows of cordierite porphyroblasts. Figure 6f shows mineral composition changes across the isograd. The minerals are Mg-rich as expected (e.g. Mg/(Mg + Fe) of cordierite = 0.82–0.90). Although there is overlap, biotite is Mg-richer in some of the higher grade Ms + Sil + Bt assemblages than in the lower grade Ms + Crd + Sil + Bt-bearing assemblages, consistent with the isograd and textural evidence for growth of Sil + Bt at the expense of Ms + Crd.

The above data only provide constraints on the slope of reaction 1 if the metamorphic field gradient and *P–T* path of individual samples is known. The samples in Fig. 6f are separated by about 500 m vertically, corresponding to a pressure difference of about 0.15 kbar, whereas the temperature difference between the samples, based on mineral assemblages in interlayered "normal" pelite, is about 30–50 °C (Cheney & Guidotti, 1979; Cheney, 1975), giving a metamorphic field gradient of about 60–100 °C km^{-1} (*c.* 200–300 °C $kbar^{-1}$). This is consistent with a small flat to positive slope for the metamorphic field gradient. Further evidence in support of a nearly flat slope for the metamorphic field gradient is the trend to Fe-enrichment in the mineral assemblage Ms + Grt + Bt + Sil in interlayered rocks from the same interval (ΔMg/(Mg + Fe) = −0.03 and −0.01 in biotite and garnet, respectively). According to calculated isopleths of Spear & Cheney (1989) and Holland & Powell (1998), this constrains the slope of the metamorphic field gradient to 200–350 °C/kbar. Guidotti *et al.* (1986) argued that the *P–T* path is similar to the metamorphic field gradient. Although the uncertainties in the metamorphic field gradient and *P–T* path limit quantitative estimates of the slope of reaction 1, the data are more consistent with a negative slope for reaction 1 than a positive slope. Another example of a regional setting in which cordierite is inferred to give way to biotite and sillimanite by reaction 1 is the Moldanubian metapelites, Northern Bavarian Forest, Germany (Blümel & Schreyer, 1976), although whether this setting demonstrates a negative slope for reaction 1 also depends on more precise knowledge of the metamorphic field gradient than is provided.

Kyanite bearing settings

There are a small number of localities that report coexisting kyanite and cordierite in Ms + Bt-bearing schists, including the Truchas Peaks area, New Mexico (Grambling, 1981) and the Whetstone Lake area, Ontario (Carmichael *et al.*, 1978). Such localities are potentially important because, if the Ky + Crd + Ms + Bt assemblages represent a stable association, they imply that reactions 1 and 8 extend into the kyanite stability field. Such high pressure occurrences of the assemblage are expected to be particularly Mg-rich, which is generally consistent with the compositional data from these areas (Table 1).

Although Grambling (1981) interpreted the Truchas Ky + Crd + Ms + Bt assemblages to represent a stable association formed in a single metamorphic event, more recent investigations in this and other nearby areas favour a polymetamorphic history (Daniel *et al.*, 1992; Williams & Karlstrom, 1996). In this scenario, the Ky + Crd schists may have formed from a low pressure metamorphic overprint of a pre-existing regional kyanite-bearing assemblage, with cordierite forming in the low pressure overprint.

At Whetstone Lake, uncertainty about the stability of Ms + Bt + Ky + Crd in the reported assemblage is introduced because muscovite (and chlorite) are texturally 'late' (Carmichael *et al.*, 1978). Al_2SiO_5 + Crd can coexist stably to higher pressures in muscovite-free assemblages than in muscovite-bearing ones (see reaction 3 in Fig. 1a). Chlorite in these rocks plots on the Mg-rich side of the Crd-Bt tie line, at variance with other localities covering a wide range of compositions in which Chl plots on the Fe-rich side of the Crd-Bt tie line (Guidotti *et al.*, 1975; Pattison, 1987), possibly suggesting some degree of chemical disequilibrium in the rocks. As with Truchas, the possibility of polymetamorphism at Whetstone Lake cannot be ruled out.

In summary, we are uncertain that the Truchas Peaks and Whetstone Lake occurrences of Ky + Crd + Ms + Bt represent a stable association. Massonne (1989) and Reinhardt (1992; pers. comm. 2001) have argued that this association is unlikely to be stable because the [Kfs] invariant point in KMASH (Fig. 1a), which is the high pressure terminus of reactions 1 and 8 (Fig. 1b), must lie below the MASH invariant point involving Chl + Crd + Al_2SiO_5 + H_2O + Qtz + talc. Massonne (1989) located this MASH invariant point at 6.2 kbar, 620 °C, i.e. barely into the kyanite stability field, leaving little if any room for a stable Ky + Crd + Ms + Bt association.

SUMMARY OF NATURAL CONSTRAINTS

Most of the data from natural samples favours a small negative slope for reaction 1 for a wide range of Mg/(Mg + Fe) ratios in both the andalusite and sillimanite stability fields. Table 1 lists the reported Mg/(Mg + Fe) ratios of cordierite and biotite in the model univariant KFMASH assemblage Ms + Chl + Crd + Bt + Als (corresponding to univariant reaction 8) and Ms + Kfs + Crd + Bt + Als (corresponding to univariant reaction 5). Because these two univariant curves bracket divariant reaction 1 (Fig. 1), the slope of reaction 1 can be constrained from differences in Mg/(Mg + Fe) of cordierite and biotite between the two univariant assemblages in localities where both univariant assemblages are developed in the same prograde sequence, assuming that the metamorphic field gradient is known.

In Table 1, inequalities are used where the relevant univariant assemblage was not found or analyzed, but can be constrained by the compositions of minerals in bounding divariant assemblages. Referring to Fig. 3a and assuming equilibrium, compositions of cordierite

Fig. omitted in revision

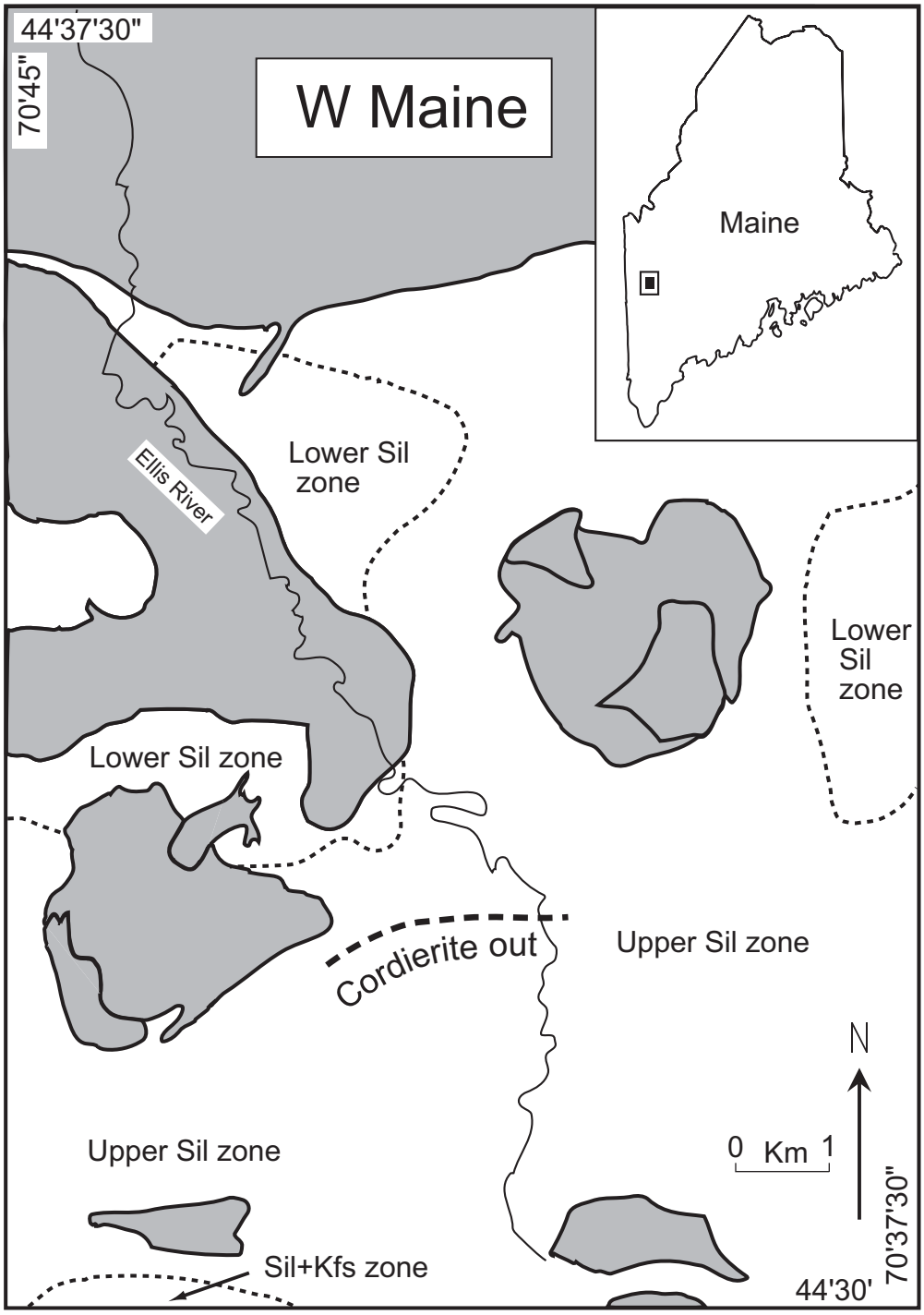

and biotite involved in divariant reactions 1 (Ms + Crd + Als + Bt) and 2 (Ms + Crd + Chl + Bt) are Mg-richer than those involved in univariant reaction 8 (Ms + Crd + Chl + Als + Bt). For divariant reaction 4 (Ms + Chl + Als + Bt), they are Fe-richer than for reaction 8. Compositions of cordierite and biotite involved in divariant reaction 7 (Ms + Crd + Bt + Kfs) are Mg-richer than those in univariant reaction 5 (Ms + Crd + Als + Bt + Kfs). For divariant reactions 1 and 6 (Crd + Als + Bt + Kfs), they are Fe-richer than for reaction 5. In practice, the above reasoning may be complicated by variations in some or all of minor elements, fluid composition and kinetics. Some contradictory relationships were found in several localities, but these were relatively few compared to localities where the patterns were consistent.

On average, in the andalusite field, the change in Mg/(Mg + Fe) of biotite and cordierite going upgrade from reaction 8 to reaction 5 averages, respectively, >0.04 (range of -0.03 to >0.08) and >0.02 (range of -0.03–0.06), respectively. Assuming an isobaric metamorphic field gradient and *P–T* path, these changes in composition translate to a small negative *P–T* slope of reaction 1 in the andalusite field of -2 to -5 bar $^{\circ}C^{-1}$. Although scarce, the data from W Maine may indicate a slightly steeper negative slope in the sillimanite field, consistent with predictions from thermodynamics (see below).

Other points (Table 1) include: (1) the presence or absence of graphite exerts an influence on the mineral compositions, with obviously graphitic rocks containing more Mg-rich minerals (e.g. Ballachulish and Kiglapait); (2) coexisting cordierite and biotite in the reaction 5 and 8 assemblages become more magnesian as pressure increases, as expected. There is a strong, if imperfect, correlation between facies series (Pattison & Tracy, 1991) and composition; (3) the lowest pressure, and Fe-richest, reaction 5 assemblages (Ms + And + Bt + Crd + Qtz + Kfs) are from the Comrie aureole, Scotland (Mg/(Mg + Fe) in biotite = 0.31); (4) the highest pressure, and among the Mg-richest, unambiguously stable reaction 8 assemblages (Ms + Sil + Bt + Crd + Chl) are from W Maine (Mg/(Mg + Fe) in biotite and cordierite ≤ 0.76 and ≤ 0.82, respectively); (5) the most Mg-rich andalusite-bearing Ms + Als + Crd + Bt assemblages are from Mt Isa, with Mg/(Mg + Fe) in biotite and cordierite ≤ 0.80 and ≤ 0.89, respectively. These values are anomalously magnesian with respect to other andalusite-bearing localities and to the higher pressure Sil-bearing assemblages of W Maine for reasons that are unclear, but might be related to the widespread metasomatism reported in the area (Rubenach, 1992). The next most Mg-rich andalusite-bearing assemblages are from the Black Hills, with Mg/(Mg + Fe) in biotite and cordierite = 0.60 and 0.74, respectively; and (6) there are several aureoles which were metamorphosed at a pressure close to or very slightly below the intersection of And = Sil and reaction 5 (facies series 1b and 1c localities in Table 1). Non-graphitic examples include Ballachulish, Lexington N and Onawa, with Mg/(Mg + Fe) in biotite and cordierite in the range 0.35–0.42 and 0.46–0.56, respectively. Graphitic examples include Ballachulish and Tono, with Mg/(Mg + Fe) in biotite and cordierite ≥ 0.46 and ≥ 0.54–0.57, respectively. Non-graphitic settings at slightly higher pressures than the intersection of the And = Sil and reaction 5 (facies series 2a localities in Table 1) include Bugaboo and Cupsuptic, with Mg/(Mg + Fe) in biotite and cordierite in the range 0.40–0.43 and 0.56–0.59, respectively. These data are impressively consistent and provide an anchoring point for the thermodynamic modelling (see below and Appendix).

A final constraint from natural occurrences is the K_D(Fe-Mg) between cordierite and biotite (= Fe/Mg (Crd)/Fe/Mg (Bt)). Holdaway & Lee (1977) obtained a mean value of 0.54 from 101 analyses collected from the literature. Addition of 115 analyses from Ballachulish, Bugaboo and other localities (see references in Table 1) raises the mean value to 0.57 from 216 analyses. In contrast to the suggestion of van Bosse & Williams (1988), there is no evidence for a trend of K_D(Fe-Mg) with grade; the scatter of data within individual metamorphic zones far exceeds any systematic change with grade (e.g. Pattison, 1987; DeBuhr, 1999). We do not claim that there is no temperature dependence, merely that it is so small to be masked by other factors such as discussed above.

THERMODYNAMIC MODELLING

The next step is to provide a thermodynamic data set that satisfies as well as possible the natural and experimental constraints on reaction 1 and other related metapelitic phase equilibria. The Appendix explains the derivation of the data, a brief summary of which is provided here. The essence of the problem is that current thermodynamic data bases predict a positive slope for reaction 1 whereas we have argued that a negative slope seems to fit the data from natural assemblages better. We began with the Spear & Cheney (1989) and Spear (1999; unpublished) thermodynamic data set, the latter which models the Tschermak component of mica and chlorite, and varied the entropy of hydrous cordierite to achieve a slope that satisfies the data from natural assemblages. We then derived the enthalpies of cordierite and biotite end members to satisfy the consistent compositions of cordierite and biotite in natural rocks formed at the intersection of reaction 5 with the And = Sil reaction (see above and Table 1). Because the *P–T* conditions of this intersection depend on the position of the And = Sil curve, which remains controversial, two datasets were derived, one based on the Holdaway (1971) curve and one based on the Pattison (1992) curve. We then extracted chlorite enthalpies for the two datasets based on natural mineral compositions in the

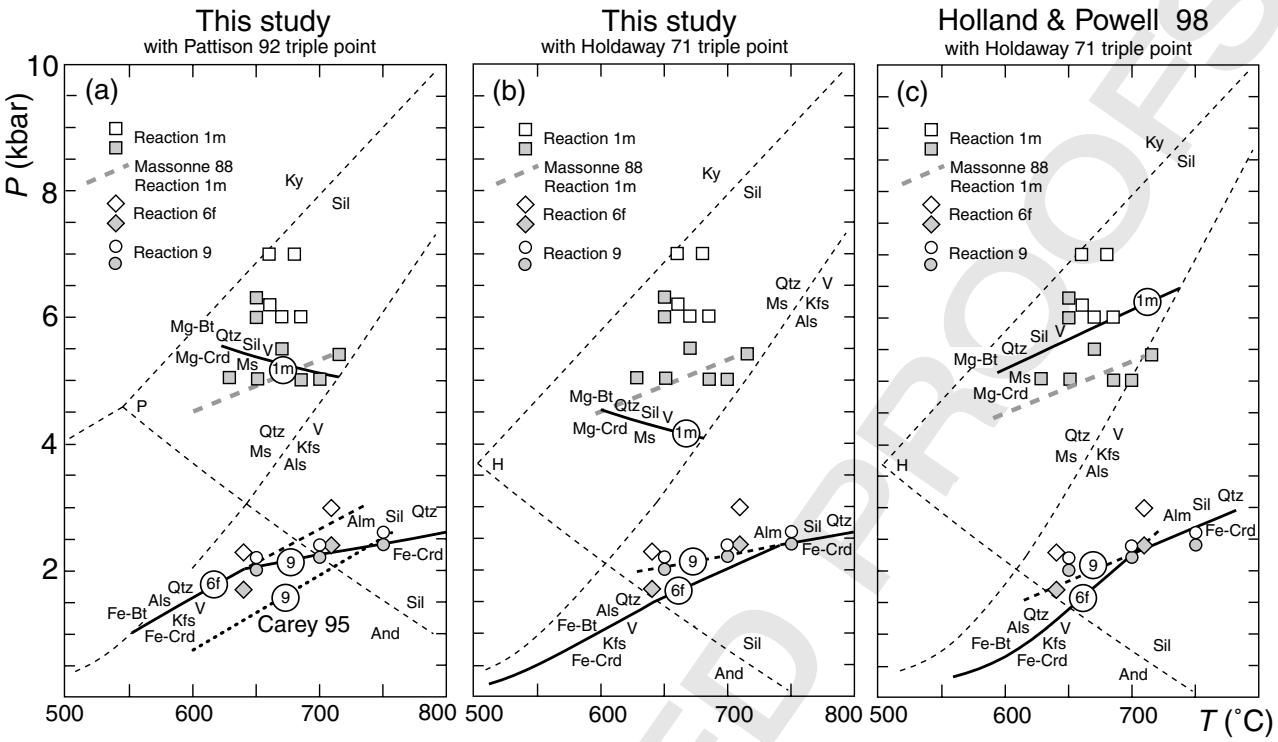

Fig. 9. Comparison of predicted reaction positions with experimental data on reactions 1m, 6f and 9. Experimental data for reactions 1m and 6f are described in Fig. 2, whereas the experimental data for reaction 9 come from Mukhopadhyay & Holdaway (1994). (a) Results of this study for the data set based on the Pattison (1992) triple point. The calculated position of reaction 9 from Carey (1995) is also shown. (b) Results of this study for the data set based on the Holdaway (1971) triple point. (c) Results using the Holland & Powell (1998) data set. See text and Appendix for discussion.

reaction 8 assemblage Ms + Chl + Qtz + Crd + And + Bt from Table 1, and finally varied almandine enthalpy to satisfy experimental constraints on reaction 9.

Figure 9 shows the experimental constraints on reactions 1m, 6f and 9 compared with calculated positions of the reactions using the two data sets of this study and the Holland & Powell (1998) data set. The Gibbs method software of Spear (1988; Spear, 1990) was used to calculate the reaction boundaries. Solid solution (i.e. Tschermak content) in the mica and chlorite is incorporated in the calculated reactions. Calculated reaction positions using the data set based on the Pattison (1992) And = Sil curve seem to fit the experimental constraints better than using the data set based on the Holdaway (1971) And = Sil curve, although a perfect fit cannot be achieved in either case (see Appendix for further discussion).

CALCULATED PETROGENETIC GRIDS

Figure 10 shows calculated petrogenetic grids in which the divariant field for reaction 1 is shaded and isopleths of Mg/(Mg + Fe) in biotite are labelled. There are two pairs of grids in Fig. 10, one pair (Fig. 10a,b) based on the Pattison (1992) And = Sil curve, the other pair (Fig. 10c,d) based on the Holdaway (1971) And = Sil curve. We emphasize that because the thermodynamic data and resultant petrogenetic grids in Fig. 10 are explicitly tied to a choice of And = Sil curve, it is invalid to use a different placement of the And = Sil curve than the one shown on each grid.

Figure 10a,c is for an assumed a_{H_2O} of 1.0, whereas Fig. 10b,d is calculated for a C–O–H fluid in equilibrium with graphite using the rationale and expressions of Connolly & Cesare (1993). No correction was made for CO_2, CH_4 and perhaps other species in cordierite (Kolesov & Geiger, 2000).

The effect of graphite on the fluid composition, and thus the relative displacement of the isopleths, increases as pressure decreases and a_{H_2O} in C–O–H fluids decreases (Connolly & Cesare, 1993). Whereas the KMASH end member reaction 1m is negligibly displaced in Fig. 10b,d compared to Fig. 10a,c, the KFASH end member reaction 1f intersects reaction 5 at about 1 kbar for pure water grid in Fig. 10a but does not intersect reaction 5 at all in the graphite grid in Fig. 10b. Isopleths are also increasingly displaced as pressure decreases: using either the Pattison-based or Holdaway-based grids, Mg/(Mg + Fe) in cordierite and biotite at the intersection of reaction 5 and And = Sil is about 0.1 higher in the graphite grid compared to the pure water grid. All of the petrogenetic grids in Fig. 10 show no stability field for Ms + Crd + St + Bt, consistent with the arguments of Pattison *et al.* (1999).

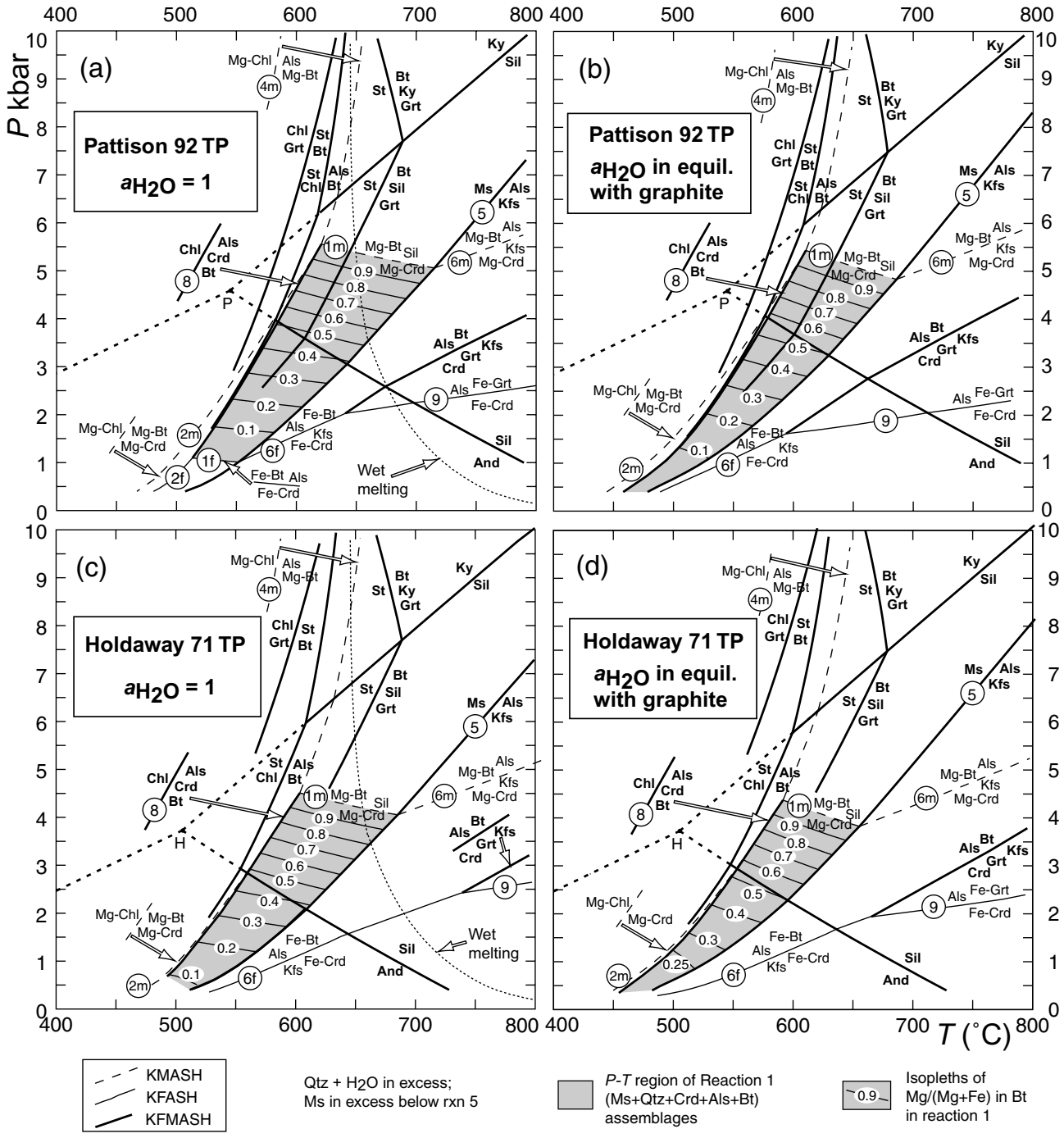

Fig. 10. Calculated metapelitic grids using the two thermodynamic data sets derived in this study and the Gibbs software of Spear (1988; 1990). (a) and (b) are calculated using the data set based on the Pattison (1992) And = Sil curve, whereas (c) and (d) are calculated using the data set based on the Holdaway (1971) And = Sil curve. Because the petrogenetic grids are explicitly tied to a choice of And = Sil curve, it is invalid to use a different placement of the And = Sil curve than the ones shown on each grid. (a) and (c) are for a pure water vapour phase, whereas (b) and (d) are for hydrous fluid in equilibrium with graphite (see text for discussion). The Fe-Mg divariant interval for reaction 1 is shaded, and contours of Mg/(Mg + Fe) in biotite through this interval are labelled. H and P — And = Sil curves and triple points of Holdaway (1971) and Pattison (1992), respectively.

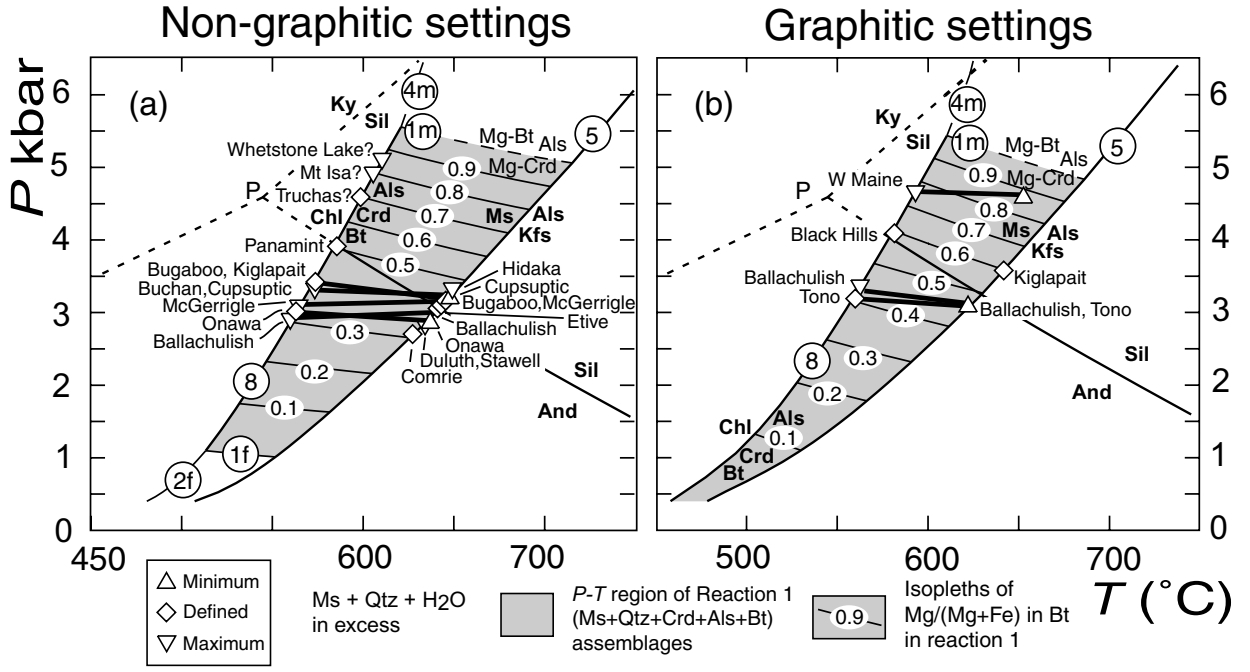

Fig. 11. Compositional data from different localities in Table 1 plotted on Fig. 10(a,b). See text for discussion of the symbols. Bold tie lines connect assemblages on reactions 5 and 8 from individual localities. P — And = Sil curve and triple point of Pattison (1992).

COMPARISON WITH NATURAL DATA

Figure 11 shows the natural localities from Table 1 plotted on the grids of Fig. 10a,b. The relative plotting positions are the same if plotted on the grids of Fig. 10c,d, but the absolute pressures are about 1 kbar lower. Upward or downward pointing symbols indicate that the compositional data provide lower or upper limits to the compositions of the minerals on the reactions in question (see earlier discussion). Diamond symbols are for rocks containing the complete reaction assemblage. Solid tie lines join compositions of minerals from individual localities that develop both of the reaction 8 and 5 assemblages. Some of the sloping tie lines connect data that are either maxima or minima, so that some degree of nonhorizontality is expected. Nevertheless, most of the tie lines are close to flat, consistent with an isobaric metamorphic field gradient.

The relative plotting positions with respect to the facies series scheme of Pattison & Tracy (1991) is good, with facies series 1 sequences (in which sillimanite first occurs upgrade of reaction 5) consistently Fe-richer than facies series 2 sequences (in which sillimanite is developed upgrade of andalusite but downgrade reaction 5). With the exception of the Mt. Isa area, the most Mg-rich andalusite-bearing Ms + Crd + Als + Bt assemblages (Panamint and Black Hills) plot near the And = Sil curve. The facies series 3 Ms + Crd + Sil + Bt assemblages of W Maine plot in the sillimanite field at about 4.5 kbar. The cordierite-out isograd in W Maine is consistent with the topology of Fig. 11b. The enigmatic Ky-bearing Truchas and Whetstone Lake areas are plotted with question marks, but occur at relatively high pressure as expected.

The predicted compositional difference between nongraphitic and graphitic assemblages also finds support in the natural data. At Ballachulish, both nongraphitic and graphitic lithologies occur in the aureole and show significant mineral assemblage and compositional differences (Pattison, 1987), yet when plotted in Fig. 11a,b record virtually the same pressure of 3 kbar (see Pattison, 1989 for a more detailed discussion and similar result). The relatively high pressure (facies series 2b) andalusite-bearing Ms + Crd + Als + Bt assemblages from Panamint and Black Hills, though of significantly different composition, both plot near the And = Sil curve when account is taken of whether or not they are graphitic.

IMPLICATIONS FOR PRESSURE ESTIMATION IN GARNET-FREE LOW PRESSURE METAPELITES

The contoured reaction 1 fields in Fig. 10 should provide a useful means to estimate pressure in low pressure Ms + Crd + Als + Bt metapelites lacking garnet. Uncertainty in the absolute position of the isopleths remains because of uncertainty in the absolute position of the And = Sil equilibrium to which they are tied (see above). Nevertheless, relative pressures using either Fig. 10a,b, or Fig. 10c,d, still pertain.

IMPLICATIONS FOR *P–T* PATHS IN LOW PRESSURE METAPELITES

Figure 10 should also improve the interpretation of *P–T* paths in low pressure metapelites. In the grids of Spear & Cheney (1989) and Holland & Powell (1998), in which reaction 1 has a shallow to moderate positive *P–T* slope, the textural and compositional data would imply that all the contact aureoles examined have a metamorphic field gradient involving significant pressure increase over a relatively small temperature interval. For example, using the Holland & Powell (1998) grid (Fig. 9c), a pressure increase of 1–1.5 kbar over the *c.* 100 °C temperature interval between reactions 8 and 5 is implied for the Ballachulish, Bugaboo and Cupsuptic aureoles. This would correspond to an increase in depth of 3–4 km over the less than 1 km width of this interval on the ground.

An example where reaction 1 figured prominently in *P–T* path interpretation is in the Cooma complex, Australia (Vernon, 1988; Johnson & Vernon, 1995). Vernon (1988) provided microtextural evidence for replacement of Ms + Crd by And + Bt and interpreted this texture to be due to reaction 1. In light of the conflicting data regarding the slope of reaction 1, Johnson & Vernon (1995) assumed a horizontal slope, which implied a prograde *P–T* path of increasing pressure to satisfy the textural observations. When combined with evidence for an isobaric retrograde path, the result was an overall anticlockwise *P–T* path for the complex. While we do not dispute the geological reasonableness of this interpretation, a negative slope for reaction 1 permits an isobaric heating and cooling path.

ACKNOWLEDGEMENTS

DRMP offers special thanks to Ron Vernon for his encouragement and mentoring over the years. This paper stems in part from discussions with Ron going back to 1989 when he led a field trip to one of his favourite petrological stomping grounds, the Cooma Complex. We thank G. DePaoli for performing most of the mineral analyses shown in Fig. 7, T. Labotka, R. Powell, M. Rubenach and A. Speer for unearthing old compositional data, and R. Voordouw and C. Sullivan for helping to compile data. J. Ferry and J. Reinhardt provided thought-provoking reviews that led to improvements in the paper. This research was supported by NSERC Research Grant 0037233 to DRMP and NSF grant EAR–9805243 to FSS.

REFERENCES

Aranovich, L. Ya. & Berman, R. G., 1997. A new garnet-orthopyroxene thermometer based on reversed solubility in FeO-Al_2O_3-SiO_2 orthopyroxene. *American Mineralogist*, **82**, 345–353.

Berman, R. G., 1988. Internally-consistent thermodynamic data for minerals in the system Na_2O-K_2O-CaO-MgO-FeO-Fe_2O_3-Al_2O_3-SiO_2-TiO_2-H_2O-CO_2. *Journal of Petrology*, **29**, 445–522.

Berman, R. G., 1991. Thermobarometry using multi-equilibrium calculations: a new technique, with petrological applications. *Canadian Mineralogist*, **29**, 833–855.

Berman, R. G. & Aranovich, L. Y., 1996. Optimized standard state and mixing properties of minerals: I. Model calibration for olivine, orthopyroxene, cordierite, garnet and ilmenite in the system FeO-MgO-CaO-Al_2O_3-SiO_2-TiO_2. *Contributions to Mineralogy and Petrology*, **126**, 1–24.

Berman, R. G. & Brown, T. H., 1985. Heat capacity of minerals in the system Na_2O-K_2O-CaO-MgO-FeO-Fe_2O_3-Al_2O_3-SiO_2-TiO_2-H_2O-CO_2: Representation, estimation, and high temperature extrapolation. *Contributions to Mineralogy and Petrology*, **89**, 168–183.

Bird, G. W. & Fawcett, J. J., 1973. Stability relations of Mg-chlorite-muscovite and quartz between 5 and 10 kb water pressure. *Journal of Petrology*, **14**, 415–428.

Blümel, P. & Schreyer, W., 1976. Progressive regional low-pressure metamorphism in Moldanubian metapelites of the northern Bavarian forest, Germany. *Krystalinikum*, **12**, 7–30.

Boberski, C. & Schreyer, W., 1990. Synthesis and water contents of Fe^{2+}-bearing cordierites. *European Journal of Mineralogy*, **2**, 565–584.

van Bosse, J. Y. & Williams-Jones, A. E., 1988. Chemographic relationships of biotite and cordierite in the McGerrigle thermal aureole, Gaspé, Québec. *Journal of Metamorphic Geology*, **6**, 65–67.

Brace, W. F., Ernst, W. G. & Kallberg, R. W., 1970. An experimental study of tectonic overpressure in Franciscan rocks. *Geological Society of America Bulletin*, **81**, 1325–1338.

Brown, M., Rushmer, T. & Sawyer, E. W., 1995. Introduction to special section: Mechanisms and consequences of melt segregation from crustal protoliths. *Journal of Geophysical Research*, **100**, 15,551–15,563.

Carey, J. W., 1995. A thermodynamic formulation of hydrous cordierite. *Contributions to Mineralogy and Petrology*, **119**, 155–165.

Carmichael, D. M., 1978. Metamorphic bathozones and bathograds: a measure of the depth of post metamorphic uplift and erosion on the regional scale. *American Journal of Science*, **278**, 769–797.

Carmichael, D. M., Moore, J. M. & Skippen, G. B., 1978. Isograds around the Hastings metamorphic 'low'. In: *Toronto '78 Field Trips Guidebook* (eds Currie, A. L. & Mackasey, W. O.), pp. 325–346. Geological Association of Canada, St. Johns.

Cheney, J. T., 1975. Mineralogy and petrology of lower sillimanite through sillimanite + K feldspar zone pelitic schists, Puzzle Mountain area, Northwestern Maine. *PhD Thesis*, University of Wisconsin, Madison, Wisconsin, USA.

Cheney, J. T. & Guidotti, C. V., 1979. Muscovite-plagioclase equilibria in sillimanite + quartz bearing metapelites, Puzzle Mountain area, Northwestern Maine. *American Journal of Science*, **279**, 411–434.

Chenhall, B. E., Jones, B. J. & Carr, P. F., 1988. Contact metamorphism of pelitic, psammitic and calcareous sediments in the Southern Highlands of New South Wales. *Australian Journal of Earth Sciences*, **35**, 389–401.

Compton, R. R., 1960. Contact metamorphism in Santa Rosa Range, Nevada. *Bulletin of the Geological Society of America*, **71**, 1383–1416.

Connolly, J. A. D. & Cesare, B., 1993. C-O-H-S fluid compositions and oxygen fugacity in graphitic metapelites. *Journal of Metamorphic Geology*, **11**, 379–388.

Daniel, C. G., Thompson, A. G. & Grambling, J. A., 1992. Decompressional metamorphic P-T paths from kyanite-sillimanite-andalusite bearing rocks in North-Central New

Mexico. *Geological Society of America Annual Meeting — Abstracts with Program*, **24**, A264.
DeBuhr, C. L., 1999. Metamorphic petrology and mass balance analysis in the Bugaboo contact aureole. *PhD Thesis*, University of Calgary, Calgary, AB, Canada.
Dickerson, R. P. & Holdaway, M. J., 1989. Acadian metamorphism associated with the Lexington batholith, Bingham Maine. *American Journal of Science*, **289**, 945–974.
Droop, G. T. R. & Treloar, P. J., 1981. Pressures of metamorphism in the thermal aureole of the Etive Granite Complex. *Scottish Journal of Geology*, **17**, 85–102.
Geiger, C. A., Armbruster, T., Khomenko, V. & Quartieri, S., 2000. Cordierite I: The coordination of Fe^{2+}. *American Mineralogist*, **85**, 1255–1264.
Grambling, J. A., 1981. Kyanite, andalusite, sillimanite, and related mineral assemblages in the Truchas Peaks region, New Mexico. *American Mineralogist*, **66**, 702–722.
Guidotti, C. V., 1984. Micas in metamorphic rocks. In: *Micas. Reviews in Mineralogy, 13* (ed. Bailey, S. W.), pp. 357–468, Mineralogical Society of America.
Guidotti, C. V., Cheney, J. T. & Conatore, P. D., 1975. Coexisting cordierite + biotite + chlorite from the Rumford quadrangle, Maine. *Geology*, **3**, 147–148.
Guidotti, C. V., Gibson, D., Lux, D. R., De Yoreo, J. J. & Cheney, J. T., 1986. Carboniferous metamorphism on the north (upper) side of the Sebago Batholith. In: *Guidebook for Field Trips in Southwestern Maine* (ed. Newberg, D. W.), pp. 306–341, New England Intercollegiate Geological Conference, 78th Annual Meeting, Bates College.
Helms, T. S. & Labotka, T. C., 1991. Petrogenesis of Early Proterozoic pelitic schists of the southern Black Hills, South Dakota: Constraints on regional low pressure metamorphism. *Geological Society of America Bulletin*, **103**, 1324–1334.
Hensen, B. J., 1971. Theoretical phase relations involving cordierite and garnet in the system MgO-FeO-Al_2O_3-SiO_2. *Contributions to Mineralogy and Petrology*, **33**, 191–214.
Holdaway, M. J., 1971. Stability of andalusite and aluminum silicate phase diagram. *American Journal of Science*, **271**, 97–131.
Holdaway, M. J. & Lee, S. M., 1977. Fe-Mg cordierite stability in high-grade pelitic rocks based on experimental, theoretical, and natural observations. *Contributions to Mineralogy and Petrology*, **63**, 175–198.
Holdaway, M. J. & Mukhopadhyay, B., 1993. A re-evaluation of the stability relations of andalusite: thermochemical data and phase diagram for the aluminum silicates. *American Mineralogist*, **78**, 298–315.
Holdaway, M. J., Mukhopadhyay, B., Dyar, M. D., Guidotti, C. V. & Dutrow, B. L., 1997. Garnet-biotite geothermometry revised: New Margules parameters and a natural specimen data set from Maine. *American Mineralogist*, **82**, 582–595.
Holland, T. J. B., 1989. Dependence of entropy on Volume for silicate and oxide minerals: a review and a predictive mode. *American Mineralogist*, **74**, 5–13.
Holland, T. J. B. & Powell, R., 1985. An internally consistent thermodynamic data set with uncertainties and correlations: 2. Data and results. *Journal of Metamorphic Geology*, **3**, 343–370.
Holland, T. J. B. & Powell, R., 1990. An enlarged and updated internally consistent thermodynamic dataset with uncertainties and correlations: the system K_2O-Na_2O-CaO-MgO-MnO-FeO-Fe_2O_3-Al_2O_3-TiO_2-SiO_2-C-H_2-O_2. *Journal of Metamorphic Geology*, **8**, 89–124.
Holland, T. J. B. & Powell, R., 1998. An internally consistent thermodynamic data set for phases of petrological interest. *Journal of Metamorphic Geology*, **16**, 309–344.
Hudson, N. F. C., 1980. Regional metamorphism of some Dalradian pelites in the Buchan area, northeast Scotland. *Contributions to Mineralogy and Petrology*, **73**, 39–51.
Johnson, S. E. & Vernon, R. H., 1995. Stepping stones and pitfalls in the determination of an anticlockwise P-T-t-deformation path: the low-P, high-T Cooma Complex, Australia. *Journal of Metamorphic Geology*, **13**, 165–183.
Key, R. M., Phillips, E. R. & Chacksfield, B. C., 1993. Emplacement and thermal metamorphism associated with the post-orogenic Strath Ossian Pluton, Grampian Highlands, Scotland. *Geological Magazine*, **130**, 379–390.
Kolesov, B. A. & Geiger, C. A., 2000. Cordierite II: The role of CO_2 and H_2O. *American Mineralogist*, **85**, 1265–1274.
Kretz, R., 1983. Symbols for rock-forming minerals. *American Mineralogist*, **68**, 277–279.
Labotka, T. C., 1981. Petrology of an andalusite-type regional metamorphic terrane, Panamint Mountains, California. *Journal of Petrology*, **22**, 261–296.
Labotka, T. C., 1983. Analysis of the compositional variations of biotite in pelitic hornfelses from northeastern Minnesota. *American Mineralogist*, **68**, 900–914.
Labotka, T. C., Papike, J. J. & Vaniman, D. T., 1981. Petrology of contact metamorphosed argillite from the Rove Formation, Gunflint Trail, Minnesota. *American Mineralogist*, **66**, 70–86.
Labotka, T. C., White, T. C. & Papike, J. J., 1984. The evolution of water in the contact-metamorphic aureole of the Duluth Complex, northeastern Minnesota. *Geological Society of America Bulletin*, **95**, 788–804.
Lonker, S. W., 1981. The *P–T–X* relations of the cordierite-garnet-sillimanite-quartz equilibrium. *American Journal of Science*, **281**, 1056–1090.
Massonne, H.-J., 1988. Die thermische Stabilität der granulitfaziellen Paragenese Aluminosilikat + Phlogopit + Quartz im System K_2O-MgO-Al_2O_3-SiO_2-H_2O. *Fortschritte der Mineralogie*, **66**, 133.
Massonne, H.-J., 1989. The upper thermal stability of chlorite + quartz: an experimental study in the system MgO-Al_2O_3-SiO_2-H_2O. *Journal of Metamorphic Geology*, **7**, 567–581.
Massonne, H. & Schreyer, W., 1987. Phengite geobarometry based on the limiting assemblage with K-feldspar, phlogopite, and quartz. *Contributions to Mineralogy and Petrology*, **96**, 212–224.
Mukhopadhyay, B. & Holdaway, M. J., 1994. Cordierite-garnet-sillimanite-quartz equilibrium: I. New experimental calibration in the system FeO-Al_2O_3-SiO_2-H_2O and certain P-T-X_{H_2O} relations. *Contributions to Mineralogy and Petrology*, **116**, 462–472.
Newton, R. C., 1995. Simple system mineral reactions and high grade metamorphic fluids. *European Journal of Mineralogy*, **7**, 861–881.
Okuyama-Kusunose, Y., 1993. Contact metamorphism in andalusite-sillimanite type Tono aureole, Northeast Japan; reactions and phase relations in Fe-rich aluminous metapelites. *Bulletin of the Geological Survey of Japan*, **44**, 377–416.
Pattison, D. R. M., 1987. Variations in Mg/(Mg + Fe), F, and (Fe, Mg) Si = 2Al in pelitic minerals in the Ballachulish thermal aureole, Scotland. *American Mineralogist*, **72**, 255–272.
Pattison, D. R. M., 1989. P-T conditions and the influence of graphite on pelitic phase relations in the Ballachulish aureole, Scotland. *Journal of Petrology*, **30**, 1219–1244.
Pattison, D. R. M., 1992. Stability of andalusite and sillimanite and the Al_2SiO_5 triple point: Constraints from the Ballachulish aureole, Scotland. *Journal of Geology*, **100**, 423–446.
Pattison, D. & Harte, B., 1985. A petrogenetic grid for pelites in the Ballachulish aureole and other Scottish thermal aureoles. *Journal of the Geological Society of London*, **142**, 7–28.
Pattison, D. R. M. & Harte, B., 1991. Petrography and mineral chemistry of pelites. In: *Equilibrium and Kinetics in Contact Metamorphism: the Ballachulish Igneous Complex and its Aureole* (eds Voll, G., Topel, J., Pattison, D. R. M. & Seifert, F.), pp. 135–180. Springer Verlag, Heidelberg.
Pattison, D. R. M. & Harte, B., 1997. The geology and evolution of the Ballachulish Igneous Complex and Aureole. *Scottish Journal of Geology*, **33**, 1–29.
Pattison, D. R. M. & Harte, B., 2001. Field guide to the Ballachulish Igneous Complex and Aureole. *Geologists'*

Association Guidebook, xx. Edinburgh University Press, Edinburgh, Scotland. in press.
Pattison, D. R. M. & Jones, J., 1993. The Bugaboo aureole: an exceptional sequence of metapelitic mineral assemblage zones. *Geological Association of Canada, Abstracts with Program*, **18**, A81.
Pattison, D. R. M., Spear, F. S. & Cheney, J. Y., 1999. Polymetamorphic origin of muscovite + cordierite + staurolite + biotite assemblages: implications for the metapelitic petrogenetic grid and for P-T paths. *Journal of Metamorphic Geology*, **17**, 685–703.
Pattison, D. R. M. & Tracy, R. J., 1991. Phase equilibria and thermobarometry of metapelites. In: *Contact Metamorphism. Reviews in Mineralogy, 26*, pp. 105–206, Mineralogical Society of America, Washington D.C.
Raeside, R. P., Hill, J. D. & Eddy, B. G., 1988. Metamorphism of Meguma Group metasedimentary rocks, Whitehead Harbour area, Guysborough County, Nova Scotia. *Maritime Sediments and Atlantic Geology*, **24**, 1–9.
Raeside, R. P. & Jamieson, R. A., 1992. Low pressure metamorphism of the Meguma Terrane, Nova Scotia. Geological Association of Canada — Mineralogical Association of Canada Joint Annual Meeting, Wolfville '92, Field Excursion Guidebook, C-5.
Reinhardt, J., 1992. Low-pressure, high-temperature metamorphism in a compressional tectonic setting: Mary Kathleen Fold Belt, northeastern Australia. *Geological Magazine*, **129**, 41–57.
Reinhardt, J. & Rubenach, M. J., 1989. The temperature-time relationships across metamorphic zones: Evidence from porphyroblast-matrix relationships in progressively deformed metapelites. *Tectonophysics*, **158**, 141–161.
Rubenach, M. J., 1992. Proterozoic low-pressure/high pressure metamorphism and an anti-clockwise P-T-t path for the Hazeldene area, Mount Isa Inlier, Queensland, Australia. *Journal of Metamorphic Geology*, **10**, 333–346.
Rutter, E. H., 1976. The kinetics of rock deformation by pressure solution. *Philosophical Transactions of the Royal Society of London, Series a: Mathematical and Physical Sciences*, **283**, 203–219.
Ryerson, F. J., 1979. Phase equilibria in the contact aureole of the Cupsuptic pluton. *PhD Thesis*, Brown University, Providence, RI, USA.
Seifert, F., 1970. Low-temperature compatibility relations of cordierite in haplopelites of the system K_2O-MgO-Al_2O_3-SiO_2-H_2O. *Journal of Petrology*, **11**, 73–99.
Shiba, M., 1988. Metamorphic evolution of the southern part of Hidaka Belt, Hokkaido, Japan. *Journal of Metamorphic Geology*, **6**, 273–296.
Shimizu, I., 1995. Kinetics of pressure solution creep in quartz; theoretical considerations. In: *Influence of Fluids on Deformation Processes in Rocks. Tectonophysics, 245* (eds Spiers, C. J. & Takeshita, T.), 121–134.
Skippen, G. B. & Gunter, A. E., 1996. The thermodynamic properties of H_2O in magnesium and iron cordierite. *Contributions to Mineralogy and Petrology*, **124**, 82–89.
Spear, F. S., 1988. The Gibbs method and Duhem's theorem: The quantitative relationships among P, T, chemical potential, phase composition and reaction progress in igneous and metamorphic systems. *Contributions to Mineralogy and Petrology*, **99**, 249–256.
Spear, F. S., 1990. Petrologic determination of metamorphic pressure-temperature-time paths. In: *Metamorphic pressure-temperature-time paths. 28th International Geological Conference — Short Course in Geology, 7, Washington, D.C.* (eds Spear, F. S. & Peacock, S. M), pp. 1–55.
Spear, F. S., 1999. Real-time AFM diagrams on your Macintosh. *Geological Materials Research*, **1**, 1–18.
Spear, F. S. & Cheney, J. T., 1989. A petrogenetic grid for pelitic schists in the system SiO_2-Al_2O_3-FeO-MgO-K_2O-H_2O. *Contributions to Mineralogy and Petrology*, **101**, 149–164.
Speer, J. A., 1981. The nature and magnetic expression of isograds in the contact aureole of the Liberty Hill pluton, South Carolina: Part II. *Geological Society of America Bulletin*, **92**, 1262–1358.
Speer, J. A., 1982. Metamorphism of the pelitic rocks of the Snyder Group in the contact aureole of the Kiglapait layered intrusion, Labrador: Effects of buffering partial pressures of water. *Canadian Journal of Earth Sciences*, **19**, 1888–1909.
Symmes, G. H. & Ferry, J. M., 1995. Metamorphism, fluid flow and partial melting in pelitic rocks from the Onawa contact aureole, central Maine, U.S.A. *Journal of Petrology*, **36**, 587–612.
Thompson, P. H., 1978. Archean regional metamorphism in the Slave structural province — A new perspective on some old rocks. In: *Metamorphism in the Canadian Shield*. (eds Fraser, J. A. & Heywood, W. W.) *Geological Survey of Canada Paper, 78–10*, pp. 85–103.
Vernon, R. H., 1988. Sequential growth of cordierite and andalusite porphyroblasts, Cooma Complex, Australia: Microstructural evidence of a prograde reaction. *Journal of Metamorphic Geology*, **6**, 255–269.
White, R. W., Powell, R., Holland, T. J. B. & Worley, B. A., 2000. The effect of TiO_2 and Fe_2O_3 on metapelitic assemblages at greenschist and amphibolite conditions: mineral equilibria calculations in the system K_2O-FeO-MgO-Al_2O_3-SiO_2-H_2O-TiO_2-Fe_2O_3. *Journal of Metamorphic Geology*, **18**, 497–512.
Williams, M. L. & Karlstrom, K. E., 1996. Looping P-T paths and high-T, low-P middle crustal metamorphism: Proterozoic evolution of the southwestern United States. *Geology*, **24**, 1119–1122.
Xu, G., 1993. Phase relationships in metapelitic rocks, with applications to metamorphism in the contact aureole of the Stawell granite, western Victoria, Australia. *PhD Thesis*, University of Melbourne, Parksville, Victoria, Australia.
Xu, G., Powell, R., Wilson, C. J. L. & Will, T. M., 1994. Contact metamorphism around the Stawell granite, Victoria, Australia. *Journal of Metamorphic Geology*, **12**, 609–624.

Received 5 January 2001; revision accepted 19 June 2001

APPENDIX: DERIVATION OF THERMODYNAMIC DATA

The desired goal was to derive a set of internally consistent thermodynamic data that would correctly predict the natural phase relations and element partitioning for low and medium pressure metapelites documented in this paper, Pattison *et al.* (1999) and Pattison & Tracy (1991 and references therein), as well as for as much of the pertinent experimental data as possible.

The starting point in the data derivation was the thermodynamic data base of Spear & Cheney (1989; Spear, 1999 and unpubl.), itself based on the data base of Berman (1988). For phases with well-calibrated thermodynamic properties, reference state entropies and volumes as well as heat capacities, expansion and compressibility values were adopted directly from the compilation of Berman (1988, 1991). Heat capacities for some end members (e.g. aluminous biotite, celadonite and chlorite) were calculated from the fits of Berman & Brown (1985), and expansion and compressibility values were assumed to be identical to other end members in the same phase. Entropies and volumes of remaining end-members were calculated as oxide sums from the fits of Holland (1989).

Enthalpies for minerals in the KASH system including quartz, K-feldspar, muscovite (Mg and Fe free), pyrophyllite, kyanite and sillimanite were adopted directly from Berman (1988, 1991), as was the entropy and volume of andalusite. Two values for the enthalpy of andalusite were used, one from Berman (1988) based on the Holdaway (1971) triple point, and another

derived to conform to a value for the Al_2SiO_5 triple point of 550 °C, 4.5 kbar, following arguments by Pattison (1992) and below.

Entropies and volumes of the Mg and Fe celadonite components in muscovite were adjusted from the oxide sum values to achieve consistency with the experimental study of Massonne & Schreyer (1987). Enthalpies of the celadonite end members were then calculated to achieve an 8 °C offset of the muscovite dehydration reaction at 3 kbar to fit these data (Spear & Cheney, 1989). Although imprecise, the small celadonite concentrations in muscovite at low pressure (<10 mole per cent) do not result in large uncertainties.

Slope of reaction 1

Several different approaches were attempted to achieve a negative slope for reaction 1. The uncertainty in entropies and volumes of biotite end members and their mixing behaviour (Holland & Powell, 1998), combined with the compositional complexity of natural biotite, makes this mineral a logical target for modification. However, repeated attempts at creating a grid that conformed to observed low-pressure phase relations as well as various experimental constraints by changing only these parameters routinely failed. In particular, although the S of biotite end members could be modified to achieve a negative slope for reaction 1, when additional experimental constraints were applied to compute enthalpies of cordierite, biotite, chlorite and garnet, unacceptably large discrepancies between calculated and observed Fe-Mg partitioning between biotite and these phases ensured. Additional efforts were expended exploring the consequences of decreasing the entropies of cordierite end members. For example, decreasing the entropy of Mg cordierite to 372 J mole-K^{-1} produced the desired slope for reaction 1, but resulted (Spear, 1999; unpublished) in incorrectly predicting a sizeable stability field for staurolite + cordierite + muscovite + biotite and incorrect Fe-Mg partitioning between biotite and cordierite.

We then turned our attention to the thermodynamics of cordierite hydration. Carey (1995), Newton (1995) and Skippen & Gunter (1996) provided the most recent thermodynamic fits to a large body of experimental hydration data listed and described in these papers. The Carey model is similar to the one used by Holland & Powell (1998) and Spear (1999 and unpubl.), and gives an entropy of water in cordierite of 81 J K-mol^{-1}.

In evaluating his model against reaction 9, Fe-Crd → Alm + Sil + Qtz, Carey found that the calculated slope was steeper than the precise experimental brackets of Mukhopadhyay & Holdaway (1994) (Fig. 7 of Carey, 1995 and Fig. 9a of this paper). A similar, although less extreme, disparity in slope between the calculated position of reaction 9 and the constraining experiments is also found using the data base of Holland & Powell (1998) (Fig. 9c). Because the entropy and volume of the other phases in the reaction are relatively well known, the chief determinant of the slope of reaction 9 is the thermodynamic model for water in cordierite. Progressive reduction of the entropy of water in cordierite flattens out the slope of reaction 9 while at the same time rotates the slope of reaction 1 from positive to flat to gently negative. A value of 50 J K-mol^{-1} results in a slope for reaction 9 that optimally matches the slope indicated by the experimental brackets and additionally rotates reaction 1 to a shallow negative slope that provides a good fit to the natural data (see main text). Accepting this value, we then calculated the enthalpy of hydration to be consistent with an $X(H_2O)$ in cordierite of 0.6 at 640 °C, 3.0 kbar, a value that is well constrained by the experimental data (Fig. A1).

The resulting isopleths for $X(H_2O)$ in cordierite are shown in Fig. A1. The mismatch with experiments is largest below 600 °C. However, our model fits the experiments adequately over the *P–T* range in which cordierite is stable (Fig. A1). Considering the significant uncertainties in the hydration experiments (see discussions in Lonker, 1981 and Carey, 1995) and the possibility

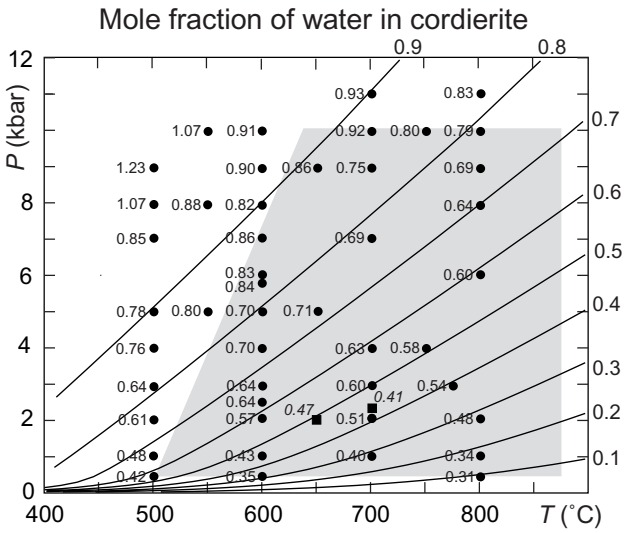

Fig. A1. *P–T* diagram showing isopleths of the mole fraction of water in cordierite (solid lines) from the model used in this study (see Appendix for discussion). The hydrous end member is assumed to contain 1.0 mole of water. The experimental data (solid circles) are from Table 1 of Carey (1995), with multiple values at individual *P–T* points averaged, whereas the solid squares are data from Mukhopadhyay & Holdaway (1994). The grey screen is the approximate *P–T* limit for cordierite in metapelites.

that natural cordierite contains additional channel-filling species that may affect the thermodynamics of water in cordierite (Geiger *et al.*, 2000; Kolesov & Geiger, 2000), we consider our hydration model to be a reasonable compromise. The hydration effects in Fe-cordierite are assumed to be the same as in Mg-cordierite (Boberski & Schreyer, 1990; Mukhopadhyay & Holdaway, 1994; Skippen & Gunter, 1996).

Position of reaction 1 and its dependence on the position of the And = Sil equilibrium

Having established the entropy and enthalpy of hydration of cordierite, absolute enthalpies for Mg and Fe cordierite, phlogopite, annite, eastonite, and siderophyllite were calculated by using natural assemblage data as a reference (Table 1 and K_D (Fe-Mg) between cordierite and biotite). This approach is justified by the generally consistent variation in the compositions of the natural minerals as a function of pressure (Table 1). Using natural samples as references for calculation of thermodynamic properties ensures conformity of the resultant grid with natural parageneses, which is the goal of the exercise.

Of particular importance are the several natural settings metamorphosed at a pressure at or near the intersection of reaction 5 and And = Sil, all of which show similar mineral compositions: Mg/(Mg + Fe) in Bt and Crd = 0.38 ± 0.03 and 0.51 ± 0.05, respectively (Table 1). Because of this consistency, we accept this as the principal anchoring point in our calculation of the cordierite and biotite enthalpies.

A complication in this approach is uncertainty in the position of the And = Sil equilibrium. We calculated two separate thermodynamic sets assuming the Holdaway (1971) and Pattison (1992) positions of the And = Sil equilibrium. For the Holdaway curve, reaction 5 intersects And = Sil at 2.1 kbar, 600 °C, whereas for the Pattison curve the intersection is at 3.0 kbar and 640 °C. The mineral compositional parameters used as input data for each data set are identical and are listed in Table A1. The enthalpy of almandine in both data sets was

Table A1. Reference assemblage and mineral compositions for calculation of cordierite and biotite enthalpies.

T	640 °C (Pattison triple point) or 600 °C (Holdaway triple point)
P	3.0 kbar (Pattison triple point) or 2.1 kbar (Holdaway triple point)
Quartz	SiO_2
Andalusite	Al_2SiO_5
K-feldspar	$KAlSi_3O_8$
Fluid	H_2O
Muscovite*	K $(Mg_{0.035}Fe_{0.035}Al_{1.93})$ $(Si_{3.07}Al_{0.93})$ $O_{10}(OH)_2$
Biotite	K $(Mg_{0.72}Fe_{1.28})$ $(Mg_{0.25}Fe_{0.35}Al_{0.40})$ $(Si_{2.60}Al_{1.40})$ $O_{10}(OH)_2$ $Mg/(Mg+Fe) = 0.37$
Cordierite	$(Mg_{1.02}Fe_{0.98})$ $Al_4Si_5O_{18}$* 0.60 H_2O $Mg/(Mg+Fe) = 0.51$

*Calculated values.

then adjusted to preserve consistency with the experiments of Mukhopadhyay & Holdaway (1994).

The results of the two approaches are compared against the experimental data on reactions 1m, 6f and 9 in Fig. 9a,b. The data set based on the Pattison triple point allows for a reasonable fit to most of the experimental data, although the position of reaction 1m is 0.5–1.0 kbar below the position implied by the experimental brackets of Seifert (1970) and Bird & Fawcett (1973). For the data set based on the Holdaway triple point, reaction 1m is 1.5–2.0 kbar below the experimental brackets and reaction 6f is about 0.5 kbar below the experimental brackets. If one accepts the Holdaway And = Sil curve *and* the experimentally determined positions of reactions 1m and 6f (see Fig. 2a), the Mg/(Mg + Fe) of biotite in the assemblage Ms + Crd + Bt + Als + Kfs + Qtz at the intersection of And = Sil and reaction 5 is predicted to be less than 0.2, significantly more Fe-rich than anything found in nature. For these reasons, we favour the data set tied to the Pattison triple point. Neither data set results in a slope for reaction 1 that agrees with the slope quoted in the unpublished experimental study of Massonne (1988), although the position of reaction 1 using the data set based on the Pattison And = Sil curve is closer to the Massonne placement than the one calculated using the Holdaway And = Sil curve.

Enthalpies of chlorite end-members were calculated in a similar manner by using reference chlorite compositions in the reaction 8 assemblage Ms + Chl + Qtz + Crd + And + Bt based on the natural data in Table 1, in particular Bugaboo (Table A2). The reference *P–T* conditions for the Pattison triple point-based and Holdaway triple point-based data sets are listed in Table A2. The compositions of all phases other than chlorite in Table A2 were calculated by the Gibbs method (Spear, 1988; Spear, 1990) using the previously determined thermodynamic data. At 3.0 kbar (Table A3), the temperature for the reaction 8 assemblage using the Pattison triple point–based data set is calculated to be 563 °C, within the range of 550–570 °C for the location of reaction 8 at 3.0 kbar using the data sets of Spear & Cheney (1989; Spear, 1999) and Holland & Powell (1998). For a uniform pressure of 3.0 kbar, the modelled differences in Mg/(Mg + Fe) in biotite and cordierite between reaction 5 (3.0 kbar, 640 °C, Table A1) and reaction 8 (3.0 kbar, 563 °C, Table A3) are 0.05 and 0.04, respectively, which fit well with the compositional trends from the natural assemblages listed in Table 1. Using the Holdaway-based data set and a pressure of 2.1 kbar, the result is the same. The chlorite in Table A3 gives a Kd (Fe-Mg) between chlorite and biotite of 0.86, the same as the average of 84 natural biotite-chlorite pairs from the literature (Pattison, unpubl. data).

Possible pitfalls in the approach to extracting the thermodynamic data

(1) There could be systematic compositional differences between the natural assemblages with which we are concerned and experimental assemblages in simple chemical systems, the latter which are the basis for the Berman (1988, 1991), Spear & Cheney (1989; Spear & Cheney, 1989) and Holland & Powell (1985, 1990, 1998) thermodynamic data sets. Although it is possible that the associated energetic effects might reconcile the topological differences discussed in the main text, we can find no obvious compositional differences that might be important. The minerals of concern to this paper are relatively uncomplicated by minor elements such as Mn, Ca & Zn. White *et al.* (2000) showed that two other potentially important minor elements, Fe^{3+} and Ti, only negligibly affect the KFMASH equilibria unless in unusually high concentration. The data base used in this paper takes account of variation in the Tschermak exchange in the sheet silicates in a similar fashion to Holland & Powell (1998). We have calculated the effects of the most important factor that affects a_{H_2O} in dehydrating metapelites, graphite (Fig. 10). A remaining possibility concerns CO_2 and alkalies in natural cordierite. The effect of these species on the thermodynamics of cordierite seems to be largely unknown (Geiger *et al.*, 2000; Kolesov & Geiger, 2000), so this is an area that deserves further investigation.

(2) By selectively adjusting the thermodynamic parameters of some of the end members, the internal consistency of the starting database is upset. With regard to the thermodynamics of water in cordierite, we are not concerned with this point in principle because in the data bases of Berman (1988, 1991; Berman & Aranovich, 1996) and Holland & Powell (1985, 1990, 1998), expressions for the thermodynamic properties of water in cordierite are used as input data to the respective data extraction algorithms. This means that the thermodynamic parameters for a number of mineral end members in these databases are tied to the assumed cordierite hydration model. It should thus be possible to extract a thermodynamic database for a different assumed cordierite hydration model that provides an equally satisfactory fit to the phase equilibrium and calorimetric constraints.

We do not wish to imply that individual thermodynamic parameters for cordierite, or for other phases in the modified data

Table A2. Reference assemblage and mineral compositions for calculation of chlorite enthalpies.

T	570 °C (Pattison triple point) or 550 °C (Holdaway triple point)
P	3.3 kbar (Pattison triple point) or 2.4 kbar (Holdaway triple point)
Quartz	SiO_2
Andalusite	Al_2SiO_5
Fluid	H_2O
Muscovite*	K $(Mg_{0.02}Fe_{0.03}Al_{1.95})$ $(Si_{3.05}Al_{0.95})$ $O_{10}(OH)_2$
Biotite*	K $(Mg_{0.78}Fe_{1.22})$ $(Mg_{0.24}Fe_{0.41}Al_{0.35})$ $(Si_{2.65}Al_{1.35})$ $O_{10}(OH)_2$ $Mg/(Mg+Fe) = 0.38$
Cordierite*	$(Mg_{1.08}Fe_{0.92})$ $Al_4Si_5O_{18}$*0.73 H_2O $Mg/(Mg+Fe) = 0.54$
Chlorite	$(Mg_{1.65}Fe_{2.34})$ $(Al_{1.0})$ $(Mg_{0.28}Fe_{0.32}Al_{0.40})$ $(Si_{2.6}Al_{1.40})$ $O_{10}(OH)_8$ $Mg/(Mg+Fe) = 0.42$

*Calculated values.

Table A3. Calculated mineral compositions for reaction 8 assemblage (Ms + Chl + Crd + And + Bt + Qtz) at 3.0 kbar, using the data set for the Pattison triple point.

T	563 °C
P	3.0 kbar
Quartz	SiO_2
Andalusite	Al_2SiO_5
Fluid	H_2O
Muscovite	K $(Mg_{0.02}Fe_{0.03}Al_{1.95})$ $(Si_{3.05}Al_{0.95})$ $O_{10}(OH)_2$
Biotite	K $(Mg_{0.66}Fe_{1.34})$ $(Mg_{0.20}Fe_{0.45}Al_{0.35})$ $(Si_{2.65}Al_{1.35})$ $O_{10}(OH)_2$ $Mg/(Mg+Fe) = 0.32$
Cordierite	$(Mg_{0.94}Fe_{1.06})$ Al_4 Si_5O_{18}*0.72 H_2O $Mg/(Mg+Fe) = 0.47$
Chlorite	$(Mg_{1.41}Fe_{2.59})$ $(Al_{1.0})$ $(Mg_{0.24}Fe_{0.36}Al_{0.40})$ $(Si_{2.60}Al_{1.40})$ $O_{10}(OH)_8$ $Mg/(Mg+Fe) = 0.36$

base, are as reliable as data extracted from experiments or calorimetry. On the other hand, the existing data bases are deficient when it comes to predicting a number of key metapelitic phase relations, especially at low pressure. Our data base results in calculated low pressure metapelitic phase equilibria and attendant compositional data that provides a satisfactory fit to a large body of natural data, and should thus be useful in that context.